Summer 2020

Expansion Microscopy: A New Approach to Microscopic Evaluation

Ashley Ferri

Expansion Microscopy: A New Approach to Microscopic Evaluation

by

Ashley Ferri

Bachelor of Science
University of South Carolina, 2014

Submitted in Partial Fulfillment of the Requirements

For the Degree of Master of Science in

Biomedical Science

School of Medicine

University of South Carolina

2020

Accepted by:

Robert L. Price, Director of Thesis

Jay D. Potts, Reader

Ana Pocivavsek, Reader

Cheryl L. Addy, Vice Provost and Dean of Graduate School

ACKNOWLEDGEMENTS

I would like to extend thanks to my mentor Dr. Robert L. Price, and my thesis advisors Dr. Jay Potts, and Dr. Ana Pocivavsek. I would like to thank Mike Gore and Matthew Efrid of the University of South Carolina School of Medicine machine shop for their help in designing and creating a prototype for the new gelation chamber. I would also like to thank Nick Maxwell and Nathan Wagner for their help in identifying brain structures; and Lorain Junor and Anna Harper for their instruction and guidance in immunohistochemistry procedures and operation of the IRF equipment.

ABSTRACT

Optical microscopy resolution is limited by the wavelengths of light and the series of microscope lenses and other optical components used to create a magnified image of cell structures in a sample. Often the cell structures are smaller or closer together than the resolution limits of a light microscope. In 2015 the Boyden group at the Massachusetts Institute of Technology (MIT) created a sample preparation technique, expansion microscopy which involves embedding biological samples in a crosslinked, swellable, hydrogel polymer that allows for uniform physical separation of cell components so that they can subsequently be resolved by light microscopy. Using the protein retention variant of expansion microscopy, these experiments evaluated the efficacy of the technique. Forty-micron thick rat hippocampal specimens were labeled GFAP and NeuN antibodies to image the neurons and astrocytes within the tissue. The expansion process produced a 4.7-fold physical expansion of the hippocampal slices. The process was also evaluated using 50 – 100 um thick samples of mouse cardiac tissue, labeled to visualize the cytoskeleton, intercalated discs, and cellular nuclei. However, due to the strong structural integrity of cardiac tissue expansion was inconsistent and incompatible with cardiac tissue samples. Variations to the procedure are required to compensate for the rigidity and anisotropic nature of cardiac tissue. One challenge faced when expanding the samples was creation of a consistent and uniform expansion gel and handling of the fragile embedded tissue. To alleviate these difficulties, we designed a new gelation chamber that allowed for more consistent sample preparation.

Table of Contents

List of Tables

List of Figures

Chapter 1. BACKGROUND

Imaging of biological tissue allows scientists to learn more about the structure and function of biological systems and examine the effects of stimuli on the microstructure of those systems. In the study and analysis of biological materials, microscopy is an immensely valuable resource. Advancements in wide field fluorescence, confocal, and super resolution microscopy have allowed for more specific evaluation of the structure and function of biological tissues. Traditional microscopy techniques utilize photons of light, lenses, and detectors to enlarge the visual representation of a sample, but even under ideal conditions resolution is only 250 nm.

These advancements have achieved great success in resolving small structures and usually allow for the visualization of structures and proteins smaller than 200 nm or that are 20 nm or more apart. Although this advancement is significant, the limits of spatial resolution can still hinder the understanding of placement and function of proteins of interest. Determining whether two objects of interest are co-localized, or if they are separated by a distance that is less than the 200 nm spatial resolution limit, remains limited when imaging with standard optical microscopy systems. Various forms of super resolution microscopy includes a group of recently developed techniques that utilize unique combinations of lasers and fluorochromes in conjunction with deconvolution to resolve structures and proteins that are 20 – 30 nm apart (Feng, 2018). Table 1.1 below shows several common super resolution techniques, and the resulting lateral resolution. These super resolution techniques are very expensive to perform and are often unattainable to the every-day researcher.

Expansion microscopy is a technique invented by Edward S. Boyden and his group at the Massachusetts Institute of Technology (MIT) that can be used with conventional microscopy techniques to obtain super resolution results with conventional microscopy techniques (Truckenbrodt, et al., 2018).

Table 1.1 Super resolution microscopy techniques

Super Resolution Technique	**Lateral Resolution**
Structured Illumination Microscopy (SIM)	~ 100 nm
Stimulated Emission Depletion Microscopy (STED)	~ 30 - 70 nm
Single-Molecule Localization Microscopy (SMLM)	~ 20 nm
Photoactivated Localization Microscopy (PALM)	~ 10 - 50 nm
Stochastic Optical Reconstruction Microscopy (STORM)	~ 10 - 50 nm
Expansion Microscopy	~ 20 – 50 nm
(Schermelleh, 2019) (Galbraith, 2011)	

Whereas traditional microscopy techniques use light and lenses to magnify and image, expansion microscopy physically manipulates the sample itself, by increasing the distance between labeled components. This allows researchers to discern structures and label locations that were previously too close together to resolve. Although the resolution of the microscope is still approximately 200 nm, this expansion has been shown to produce a relative spatial resolution as small as 25 nm using traditional wide field and confocal fluorescence microscopy (Truckenbrodt, et al., 2018)

The basic premise of expansion microscopy is that the biological sample is embedded into a swellable hydrogel polymer; after embedding the polymer is saturated with water which causes the sample to physically swell. This pulls the labels apart and increases the distance between structures so that they can be resolved with standard widefield fluorescence microscopy. The original development of expansion microscopy required specially made fluorophore labels that bound the sample to the gel. These labels were not readily available, and were difficult to make. The procedure has since been honed and revised to use conventional fluorophores that are readily available with the development of the "protein retention" expansion microscopy technique (ProExM); (appendix table 6.2 contains a list of commonly used fluorophores). This technique involves using a compound with an amine reactive succinimidyl ester called Acryloyl X- SE. Acryloyl X-SE modifies the amines on proteins with an acrylamide functional group (Tillberg, 2019). This fuses the labeled protein to the gel, and thus survives strong digestion with proteinase

K that is part of the expansion microscopy "digestion" step (Tillberg, 2019). Using this compound to anchor proteins to the gel allows for the use of easily obtainable labels and for post-expansion labeling, which can aid in increasing the distance between proteins of interest that may be heavily clustered (Tillberg, 2019). Although most commercially available antibodies and fluorophores are compatible with expansion microscopy, there are some that can be degraded or have severely reduced fluorescence as a result of the gel polymerization and digestion procedures. Labels that fall within the cyanine family of labels such as Cy3 and Cy5 degrade severely during the polymerization process (Asano, 2018). Along with most AlexaFluor labels, most beta barrel fluorescent proteins are compatible, but non-beta-barrel proteins are susceptible to degradation during the digestion process (Asano, 2018).

The expansion microscopy technique has also been modified, and new protocols have been developed for use in specialty analysis of nucleic acids (expansion fluorescence *in situ* hybridization) and in iterative expansion, where the sample is expanded twice for a ~20X linear increase. Iterative expansion microscopy has been used to visualize synaptic proteins in brain tissue and has been shown to have a ~ 25 nm spatial resolution (Chang, 2017). One of the newer procedures that has been developed with the theory of expansion microscopy is called microscopic analysis of the proteome, or MAP. This procedure was developed to specifically identify and analyze the proteins within a biological sample and utilizes post-expansion staining that results in more linear expansion than isotropic expansion microscopy (Enger, 2016). Figure 1.1, below illustrates the overall expansion process, as well as the general procedures of the original process for expansion microscopy, the enhanced procedure that is compatible with commercially available fluorophores, the protein retention expansion microscopy method, as well as the procedure for MAP. This infographic was adapted from the work of Enger (Enger, 2016). As the subject of this study is protein retention expansion microscopy, MAP will not be discussed in-depth.

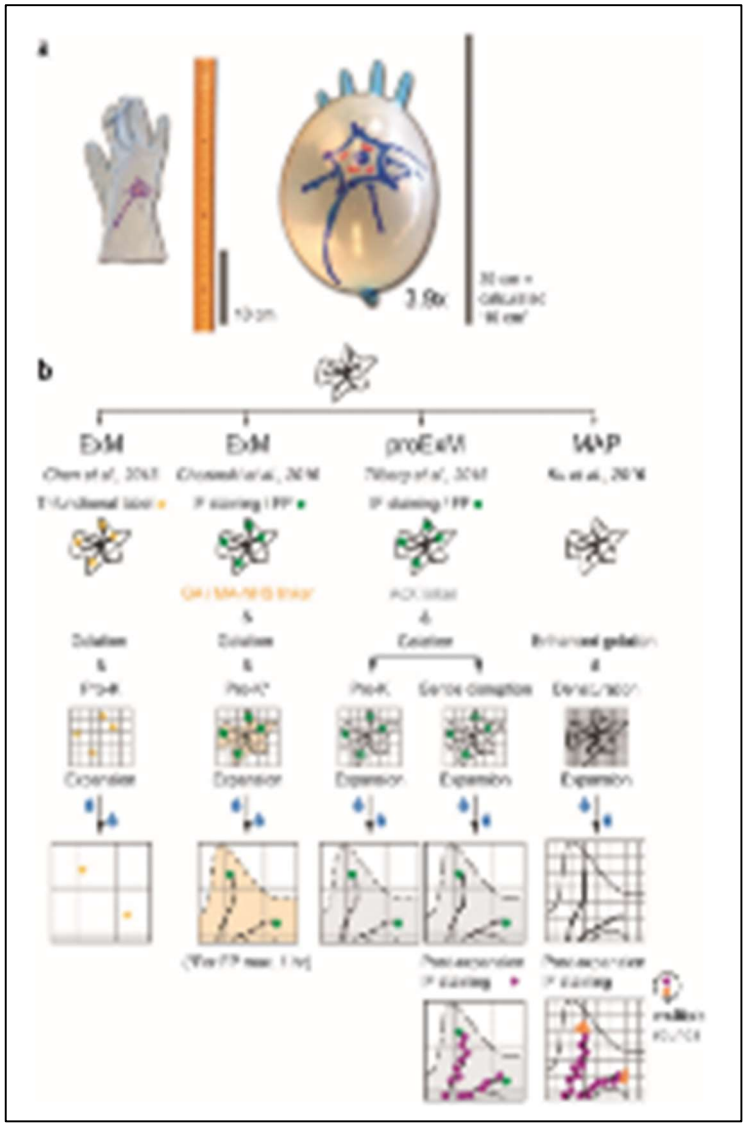

Figure 1.1. Concept and workflow of expansion microscopy techniques.
(Enger, 2016)

The advent of protein retention expansion microscopy allowed for the use of more commercially available fluorophores and for the choice of pre-expansion versus post-expansion labeling. The choice of pre or post expansion labeling allows for greater freedom in experimental development, but there are pros and cons for each technique. Labeling the sample prior to processing and expansion allows the researcher to image the sample before expanding so that the efficacy of the labeling and expansion can be judged. Expanded samples are extremely delicate and

difficult to work with so pre-expansion staining reduces the handling of expanded samples and the risk of destroying the sample prior to analysis. The expanded samples must stay hydrated to maintain their expansion. Many fluorophores can easily degrade and lose their fluorescence in water laden environment (Gao, 2017), so pre-expansion staining can help maintain the integrity of the fluorescent labels. The expansion process does increase the distance between the fluorescent labels, decreasing the concentration of label in a region of interest, and thereby decreasing the amount of fluorescence detectable by the microscope. Conversely, this increases the distance between the antibody-target epitopes, allowing for exposure of more epitopes for antibody binding and staining. This increases the concentration of the fluorescence that can be detected by the microscope. The choice of pre or post expansion staining can be vital to the success of the experiment.

The protein retention method of expansion microscopy is only one of the advancements made in the procedure since the advent of the technology. Other types of expansion microscopy include pathology-optimized expansion microscopy, iterative expansion microscopy, and expansion fluorescence in situ hybridization. The pathology-optimized form of expansion microscopy is a variation on protein retention expansion microscopy that has been adapted for use with samples that have been processed for pathology, including formalin-fixed paraffin-embedded (FFPE), hematoxylin and eosin (H&E) stained, and fresh-frozen human tissue specimens (Zhao, 2017). Processes for each type of prepared sample were created and include rehydration and antigen retrieval for FFPE samples, and the removal and re-staining of H&E samples with fluorescent antibody labels. Fresh frozen tissue samples were able to be processed using the standard protein retention expansion microscopy procedure (Zhao, 2017).

Iterative expansion microscopy is a procedure in which a sample undergoes the expansion process twice. The sample is expanded and then treated with a second swellable polymer matrix that forms in the spaces formed when the first polymer is swollen. This second matrix is then expanded again. This process can yield a 20X increase in tissue volume and achieves

approximately 25 nm relative spatial resolution. Iterative expansion microscopy has been used to image synaptic proteins and the architecture of dendritic spines (Chang, 2017).

Expansion fluorescence in situ hybridization is a method of expansion microscopy that is used to image RNA with nanoscale resolution. In this procedure, a fluorescent probe attached to complementary RNA are delivered to the desired area. After the probes are attached a reagent using an amine group and an alkylating group links a portion of the guanine molecules in the RNA to the expansion gel. After treatment with this reagent, the expansion process is performed as the normal procedure outlines. This, again, allows for the expansion of the sample, decrowding of the labels, and a greater relative spatial resolution. Although the expansion factor was found to be slightly lower than the protein retention expansion microscopy protocol, approximately 3.3 versus 4.5 times, the procedure has still proven successful in visualizing RNA in the samples (Chen F. W., 2016).

Figure 1.2 below outlines the general procedure for preparation and expansion of samples, as well as chemical linking of the sample probes to the expansion gel. Sections A-C outline the workflow for the protein retention expansion microscopy procedure with different labeling variations. Section A shows the pre expansion staining, treatment with the Acryloyl-X SE linking agent, Proteinase K digestion, and expansion processes. Section B shows the same process, but instead of pre expansion staining, these samples genetically express fluorescent proteins. Section C shows the protein retention expansion microscopy procedure utilizing post expansion staining. Section D outlines the procedure for expansion fluorescence in situ hybridization. In this procedure the label is fixed to the RNA, and the sample is gelled and digested overnight in Proteinase K. After digestion, the RNA is hybridized and then the sample is expanded. Section E details the chemical linking of the Acryloyl-X to the protein, and the binding to the guanine base of the RNA for the expansion fluorescence in situ hybridization procedure (Asano, 2018).

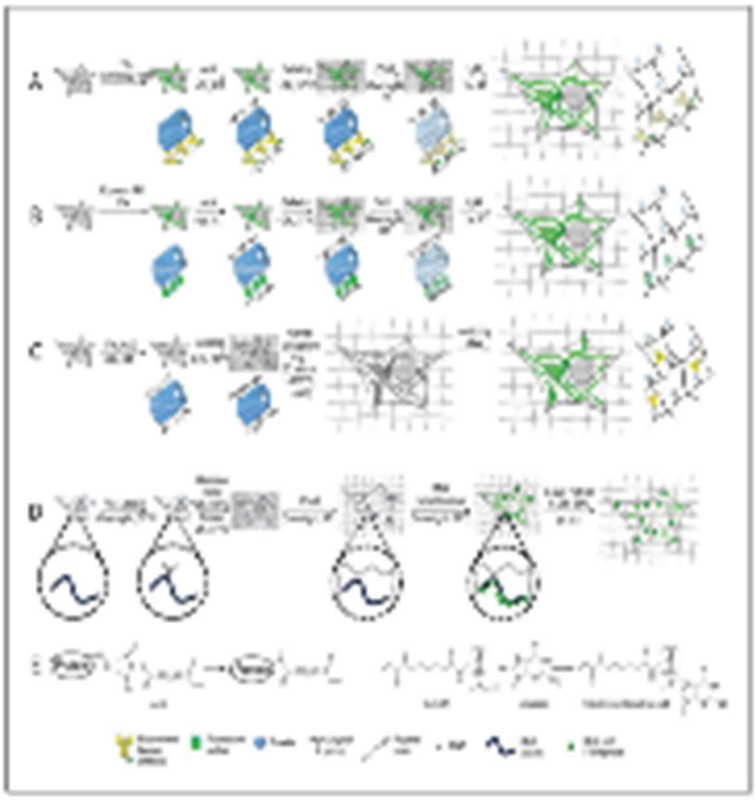

Figure 1.2 Expansion microscopy theory. (Asano, 2018)

As of June 2020, a search of PubMed with the keyword "expansion microscopy" yielded 1,863 publications since 2015. Fifty of these publications are involved experiments that used one of the forms of expansion microscopy developed by Boyden's group. These experiments were performed all over the world on samples varying from cultured cells, to pieces of tissue, to examination of whole drosophila larvae (Chang, 2017; Tsai, 2017). The purpose of my thesis is to develop protocols for expansion microscopy in the Instrumentation Resource Facility (IRF) for use in future experiments. This technique has been used by research institutions all over the world and could aid researchers in obtaining super resolution images with the readily available equipment currently in the IRF.

1.1 SPECIFIC AIMS

1.1.1 Development of a Protocol for use in the IRF

The primary purpose of this experiment was to develop an Expansion Microscopy protocol for use in the University Of South Carolina School of Medicine's Instrumentation Resource Facility. Using techniques from the paper *Expansion Microscopy: Protocols for Imaging Proteins and RNA in Cells and Tissues* from Asano, et al (2018) a protocol for performing expansion microscopy on biological tissue samples was developed. For this Specific Aim brain slices were stained with GFAP and NeuN antibodies. This protocol will serve as a standard operating procedure for the IRF to perform expansion microscopy for future experimentation and analysis.

1.1.2 Examine the ability of Protein Retention Expansion Microscopy to evaluate cellular junctions in cardiac tissue

As this technique has been primarily evaluated in neurological tissue, part of this experiment was to examine its efficacy in cardiac tissue. Although the structure of cardiac tissue is anisotropic in nature, the technique of expansion microscopy should be able to be used to examine the structure of gap junctions within the intercalated discs between muscle fibers. Since these structures are comprised of transmembrane proteins, and not rigid contractile fibers, their structure should expand isotropically within the gels (Nielsen, 2012). The intercalated discs occur between cell junctions and contain gap junctions that allow the cells to communicate. These gap junctions are made of transmembrane proteins called connexins (Pratten, 2014). These gap junctions are composed of proteins, and not contractile muscle fibers that make up other cardiac structures, so the isotropic expansion of the expansion microscopy gel should be compatible with the examination of intercalated discs.

1.1.3 Design a new gelation chamber to facilitate the creation of gelled samples

One of the more difficult and variable portions of this protocol is the construction of the gelation chamber. The gelation chamber serves to limit the amount and size of the gel to be

polymerized. If there is too much gel above or below the tissue sample, the gel may become too thick to accommodate the working distance of the microscope objective. Working with Mike Gore and Matthew Efrid of the Pharmacology Physiology and Neurosciences department, the secondary aim of this experiment was to create a new gelation chamber for use with the protein retention expansion microscopy procedure (ProExM). The goal of this design is to facilitate the creation of the gels and allow for researchers to more streamline the process of sample gelation.

Chapter 2. MATERIALS AND METHODS

2.1 DEVELOPMENT OF A PROTOCOL FOR USE IN THE IRF

*Unless otherwise specified "PBS" pertains to 1X, or 0.01M phosphate buffered saline.

*A list of chemicals used, their sources and catalog numbers can be found in Table 6.1 in the Appendix.

2.1.1 Tissue Fixation and Sectioning

Samples of adult male Wistar rat brains were obtained from the lab of Dr. Ana Pocivavsek. The animals were intracardially perfused with a 4% paraformaldehyde solution and the brains were extracted. The tissue was submerged in 30% sucrose and frozen with 2methylbutane and dry ice. Forty-micron thick coronal slices were cut on a Microm HM 560 sliding microtome, located in Dr. Susan Wood's laboratory. The samples were stored at -20^{0}C in a cryoprotectant solution of 25% ethylene glycol, 25% glycerol and 50% PBS, for two months.

2.1.2 Staining

The hippocampal region was isolated from the section for further processing. These hippocampal sections were placed into individual wells of a 12-well plate and washed 3 times for fifteen minutes per wash in PBS.

The samples were blocked for one hour in a blocking buffer of 5% normal donkey serum (NDS) and 0.4% Triton-X 100 in PBS. The samples were then incubated with 1 mL of each of the primary antibody solutions at 4^{0}C, overnight. The primary antibody solutions were a 1:500 dilution of mouse anti-NeuN monoclonal antibody (MD Millipore, lot number 3319388) in PBS, and a 1:500 dilution of rabbit anti-GFAP monoclonal antibody (Cell Signaling Technologies, reference number

12389S, lot number: 5) in PBS. After the overnight incubation, the staining solution was removed, and the samples were washed 4 times, 15 minutes per wash, with PBS. The tissues were blocked again in a 5% NDS/ 0.4% Triton X-100 mixture in PBS for one hour. The tissue samples were then incubated overnight in 1 mL of each of the secondary antibody solutions. The secondary antibody solutions were a 1:500 dilution AlexaFluor 546 donkey anti- rabbit antibody (ThermoFisher Scientific lot number: 2128963) and AlexaFluor 488 goat anti-mouse IgG (Molecular Probes, lot number: 111353). After applying the secondary antibody solutions to the wells the plate was wrapped in aluminum foil. The samples were kept away from light for the duration of the experiment and incubated at 4^0C overnight. After incubation with the secondary antibody the antibody solution was removed and the samples were washed 4 times, 15 minutes per wash, with PBS. The samples were then mounted as recorded in section 2.1.3.

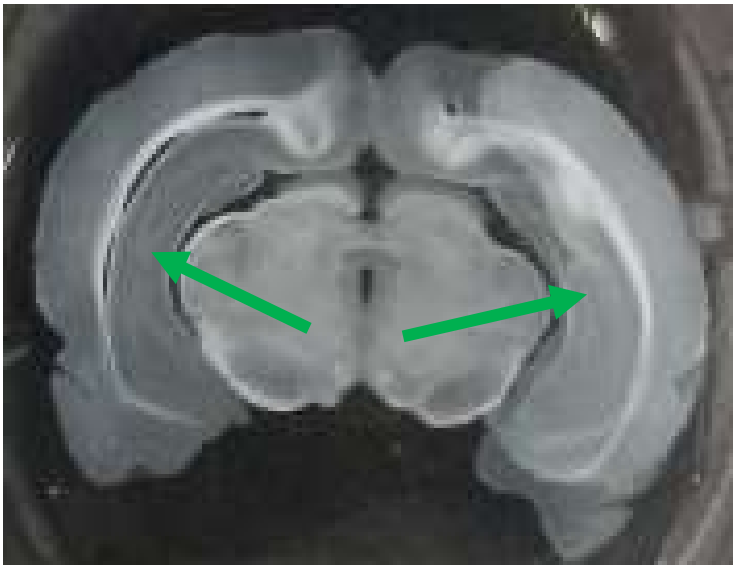

Figure 2.1 Coronal slice of rat brain tissue.

2.1.3 Pre-Expansion Imaging

Once stained, one of the tissue samples was selected and mounted on a microscope slide using a 0.1 mm thick imaging gasket and 20 – 40 uL of DABCO solution consisting of 150 mL of glycerol, 2g of DABCO (1,4-Diazabicyclo[2.2.2]octane powder (Sigma Aldrich), and 50mL of

PBS. The tissue sample was laid flat within the gasket using a soft paintbrush, and 20 - 40 uL of DABCO solution was added to the gasket. A clean microscope slide was pressed onto the gasket to seal the sample in and the slide was inverted.

The samples were imaged using the Zeiss LSM 510 META Confocal Scanning Laser Microscope (Thornwood, NY). Areas of interest were located using the 10X objective lens and the samples were imaged using Zeiss Acroplan 20X/0.50 and Zeiss Acroplan 40X/0.80 (Thornwood, NY) water immersion objectives. Samples were imaged using the 488 nm Argon Laser, the 543 nm Helium Neon Laser, a 505-530 bandpass filter for the 488 Argon laser, and a 560-615 nm bandpass filter for the 543 Helium Neon Laser. Areas of interest included regions which displayed a solid representation of staining where astrocytes (GFAP, red), and neurons (NeuN, green) were in the same area. Images were taken in two and three dimensions. Results are found in section 3.1.1 below. After imaging, the sample was removed from the imaging gasket and rinsed for 30 minutes four times each in PBS.

2.1.4 Gelation, Digestion, and Expansion

The following chemical solutions were prepared per the instructions found in appendix section 6.2; Acryloyl-X SE (AcX)/DMSO stock solution, digestion buffer (without the Proteinase K) monomer solution (Stock X), TEMED stock Solution, ammonium persulfate stock (APS), and 4-hydroxy-TEMPO solution (4HT); and stored at -20^0C. The PBS in the sample container was replaced with a 0.1 mg/mL solution of AcX in PBS, and the samples incubated at room temperature overnight with no shaking.

Two gelation chambers were constructed per the Asano protocol by gluing two 22 mm X 22mm No. 1 coverslips to a microscope slide, 22 mm apart from one another; and two 22 X 40 mm No.1 coverslips were glued together and set aside for the lid (Asano, 2018). A schematic of how the gelation chamber was constructed can be found in appendix section 6.1.5. Figure 2.2 *Manually constructed gelation chambers as described above.* shows the gelation chambers constructed per

the schematic in section 6.15. One milliliter aliquots of the following chemicals were removed from -20^0 C and thawed in an ice bath to stay cool: Stock X, 4HT, TEMED and APS.

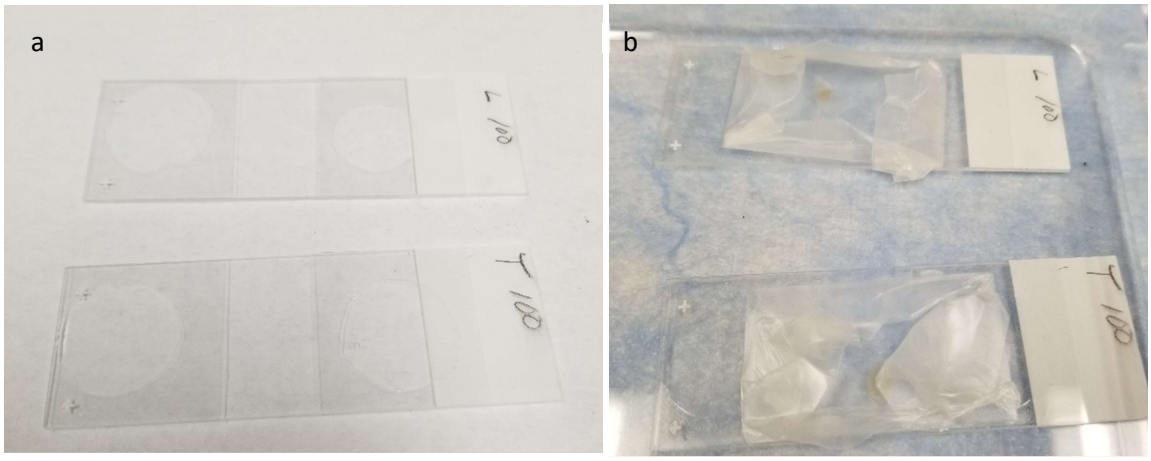

Figure 2.2 Manually constructed gelation chambers as described above.

After the overnight incubation in AcX tissues were washed twice for 15 minute each with PBS. Two mL of gelling solution were made by mixing the thawed solutions in the following ratio, on ice, in the following order (the exact amounts can be found in appendix section 6, Chemicals) 47:1:1:1, Stock X:4HT:TEMED:APS. 1 mL of gelling solution was added to each of the wells containing the samples and the sample container was placed in the freezer at -20^{0}C for 15 minutes. Samples were then moved to 4^{0}C for 15 minutes to allow the gelling solution to permeate the tissue samples.

An ice bucket was prepared, with a small flat dish to contain the gelation chambers while the next steps were performed. Since the gelling solution is extremely temperature sensitive everything was done on ice and within a 5-minute window. A droplet of 60 uL of gelling solution was added to one gelation chamber and one tissue sample was laid flat within the solution in the chamber. Another drop of solution was added to the lid of the chamber and the lid inverted and placed drop-side-down on top of the tissue sample. Using a fine-tipped pipette, 100 uL of solution at a time was added to the side of the chamber, between the lid and the base until the inside of the chamber has completely filled with gelling solution. The process was repeated with the second

gelation chamber and second tissue sample. Both chambers were placed inside an incubator at 37^0C for 2 hours to polymerize the gel.

Once the incubation was finished, the gelation chambers were removed from the incubator. Using a razorblade, the lid and side spacers were carefully removed from the microscope slide base. The excess gel around the sample was removed with the razor blade and the gel was cut asymmetrically to retain orientation for later steps. Using a soft paint brush, a small amount of digestion buffer (without Proteinase K) was painted around the outside of the gel and allowed to soak in. This loosened the gel from the base and allowed for relocation of the gelled samples. The gelled tissue samples were placed into clean wells of the 12-well plate. A digestion solution containing a 1:100 dilution of Proteinase K in digestion buffer was prepared and the solution was added to the wells containing the gelled samples. Samples were incubated at room temperature overnight.

The digestion solution was removed from the wells and the samples were transferred to 0.9 mm deep imaging gaskets that were housed in Petri dishes. Deionized water was added to the Petri dishes until it covered the gels so that the gels could absorb the water. After 20 minutes, the water was exchanged with fresh deionized water, and after another 20 minutes the water was changed again. After the three 20- minute soaks the water was removed and clean microscope slides were placed on the gaskets that held the expanded gels and pressed down to seal.

2.1.5 Post Expansion Imaging

Using the same technique as the pre-expansion imaging the samples were imaged using the Zeiss LSM 510 META Confocal Scanning Laser Microscope. Regions of interest included areas that displayed a solid representation of staining where astrocytes (GFAP, red), and neurons (NeuN, green) were in the same area. Images were taken in two and three dimensions. Results can be found in section 3.1.3 below. Once the imaging was completed, the samples were removed from

the gaskets and placed back in the Petri dishes. PBS was added to the Petri dishes to shrink and preserve the samples. These samples were kept at -4^{0}C for no more than 2 weeks.

2.2 Examination of Intercalated Discs in Cardiac Tissue

2.2.1 Tissue Fixation and Sectioning

Perfused mouse heart samples were fixed with 4% (w/v) PFA in PBS for 24 hours. The tissues were cut into 100 um thick transverse sections on the Leica VT12000 Vibratome. Tissues were stored in 0.01M PBS at 4^{0}C until needed; for the purposes of this experiment two tissue samples were used at a time.

2.2.2 Staining

Tissues were stained using an extended staining protocol to ensure the labels fully permeated the tissue. Two 100 um thick tissue samples were placed into individual wells of a 21-well plate and washed for 5 hours in a mixture of 0.01M Glycine, 0.1% Triton-X 100, and PBS to permeabilize the tissue. The tissues were blocked for 1 hour in a solution of 5% bovine serum albumin (BSA) in PBS, and for another hour in a solution of 5% NDS in 1% BSA in PBS. The primary antibody of choice for this experiment was Sigma Aldrich Anti-Connexin 43 polyclonal antibody produced in rabbit. (lot number 078M4786V). The tissue samples were incubated in a 1:100 solution of antibody diluted in a solution of 1% BSA in PBS for 48 hours at 4^{0}C with gentle shaking.

After incubation with the primary antibodies, the samples were rinsed twice for 15 minutes each rinse with 1% BSA in PBS. The tissues were then blocked again with a solution of 5% NDS in 1% BSA in PBS. After blocking, the samples were incubated for 48 hours in a 1:100 solution of secondary antibody in 1% BSA in PBS. The secondary antibody used for this experiment was Invitrogen AlexaFluor 546 donkey anti-rabbit antibody (ThermoFisher Scientific, lot number: 2128963). After applying the antibody the sample container was wrapped in aluminum foil to

protect from light and all subsequent steps were performed with foil covering the container. Once the incubation with the secondary antibody was complete the tissues underwent two 15-minute washes in 1% BSA in PBS and one 15-minute wash in PBS alone.

The tissues were then incubated for 48 hours in a 1:50 solution of Invitrogen AlexaFluor 488 Phalloidin (ThermoFisher Scientific, lot number: 1948083) in PBS, at 4^0C. After the phalloidin incubation the samples were washed 3 times for 15 minutes each with PBS; and then were incubated overnight in a 1:5000 solution of Molecular Probes 4‘,6-diamidino-phenylindole,d (DAPI) in PBS. After overnight incubation the samples were rinsed twice, for 15 minutes each, in PBS.

2.2.3 Pre-Expansion Imaging

Once stained, one of the tissue samples was selected and mounted on a microscope slide using a 0.9 mm thick imaging gasket and 80 uL of DABCO. The tissue sample was laid flat within the gasket using a soft paintbrush, and 80 uL of DABCO was added to the gasket. A clean microscope slide was pressed onto the gasket to seal the sample in and the slide was inverted.

The samples were imaged in the same way as described in section 2.1.3, but also included the use of a 405 nm diode laser and 240-480 nm bandpass filter for that laser. Regions of interest included areas which displayed a solid representation of staining where intercalated discs (connexin 43, red), cytoskeletal fibers (phalloidin, green), and cell nuclei (DAPI, blue) were present. Images were taken using a Zeiss Acroplan 20X/0.50 (Thornwood, NY) water immersion lens, in two and three dimensions. Results can be found in Section 3.2 below. After imaging, the sample was removed from the imaging gasket and rinsed for four times for 30 minutes in each rise in PBS.

2.2.4 Gelation, Digestion, and Expansion

Due to the dense nature of heart tissue, the thick tissue variation in the Asano protocol was used (Asano, 2018). The following chemical solutions were prepared per the instructions found in appendix section 6.2; Acryloyl-X SE (AcX)/DMSO stock solution, digestion buffer (without the

Proteinase K) Monomer Solution (Stock X), TEMED stock solution, ammonium persulfate stock (APS), and 4-hydroxy-TEMPO solution (4HT); and stored at -20^{0}C. The PBS in the sample container was replaced with a 0.1 mg/mL solution of AcX in 2-(N-morpholino)ethanesulfonic acid (MES) and the samples incubated at room temperature overnight with no shaking.

After the overnight incubation in AcX, tissues were washed twice in 15-minute washes with PBS. During the washes two gelation chambers were constructed as above and 1 mL aliquots of the Stock X, 4HT, TEMED and APS were removed from -20^{0}C and thawed in an ice bath to stay cool. Two milliliters of gelling solution were made by mixing the thawed solutions in the following ratio, on ice, in the following order (the exact amounts can be found in Appendix Section 6.2) 47:1.5:1:1, Stock X:4HT:TEMED:APS. One mL of gelling solution was added to each of the wells containing the samples, the container was placed in the freezer at -20^{0}C for 15 minutes, and then moved to 4^{0}C for a subsequent 30 minutes to allow the gelling solution to permeate the tissue samples.

The samples were polymerized and removed from the chambers as detailed in Section 2.1.4. A digestion solution containing a 1:100 dilution of Proteinase K in digestion buffer was mixed, and the solution was added to the wells containing the gelled samples. The samples were incubated, at room temperature, for 48 hours in the digestion solution. The solution was changed with fresh solution each day.

The digestion solution was removed from the wells and the samples were transferred to 1.7 mm deep imaging gaskets that were housed in Petri dishes. Deionized water was added to the Petri dishes until it covered the gels so that the gels could absorb the water. After 20 minutes, the water was exchanged with fresh deionized water, and after another 20 minutes, the water was changed again. After the three 20-minute soaks in deionized water, the water was removed and clean microscope slides were placed on the gaskets that held the expanded gels and pressed down to seal.

2.2.5 Post Expansion Imaging

Expanded samples were imaged in the same way, and with the same equipment, as outlined in Section 2.2.3. Areas of interest included areas which displayed a solid representation of staining where intercalated discs (connexin 43, red), cytoskeletal fibers (phalloidin, green), and cell nuclei (DAPI, blue) were present. Images were taken in two and three dimensions. Results can be found in Section 3.2 below. Once the imaging was completed, the samples were removed from the gaskets, and placed back in the Petri dishes. PBS was added to the Petri dishes to shrink and preserve the samples. These samples were kept at -4^{0}C for no more than 2 weeks.

Chapter 3. RESULTS

3.1 DEVELOPMENT OF A PROTOCOL FOR USE IN THE IRF

3.1.1 Tissue Staining

To evaluate the process of protein retention expansion microcopy, it was first necessary to establish a staining protocol for the tissue. It has been previously determined that the fluorescent labels in the cyanine family do not hold up to the expansion microscopy process (Chozinski, 2016). Thus, for this experiment the only secondary immunohistochemical labels used were AlexaFluor 546 and AlexaFluor 488. Figure 3.1 and Figure 3.2 show that the combination of the secondary antibodies with the GFAP and the NeuN primary antibodies were successful in labeling the astrocytes (red) and neurons (green) respectively.

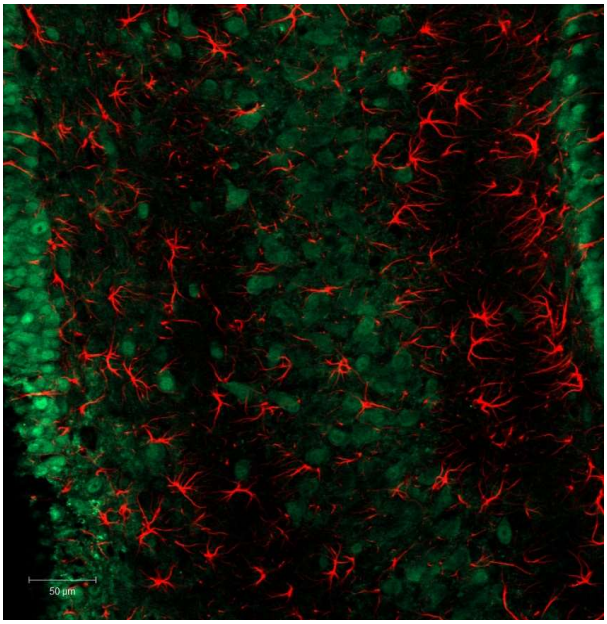

Figure 3.1. 20X image of rat hippocampus stained with NeuN and GFAP.

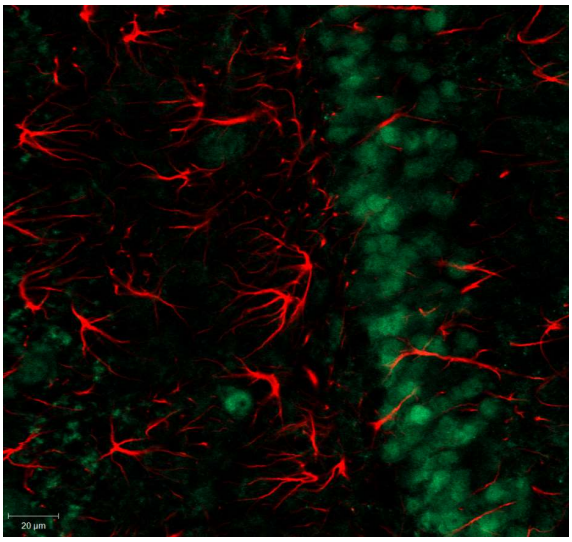

Figure 3.2. 40X Image of rat hippocampus stained with NeuN in green and GFAP.

3.1.2 Creating and expanding gelled samples

During this experiment, it was discovered that there are many steps that can be altered or adapted to the specific desired analysis. These nuances are discussed in greater detail in the Discussion Section 4.1 The following figures chronicle the process of the procedure development, some of the nuances associated with the procedure, and what can be expected while performing the ProExM procedure. Figure 3.3 and Figure 3.4 show the construction of the gelation chamber, and the chamber with the samples, prior to polymerization. Later iterations of the gelation chamber did

Figure 3.3. Early attempts at creating the gelation chamber with samples, gel and lid.

not have the parafilm cover on the lid. If the parafilm was not completely smooth, it created ridges in the gel, which made imaging and locating the area of interest more difficult.

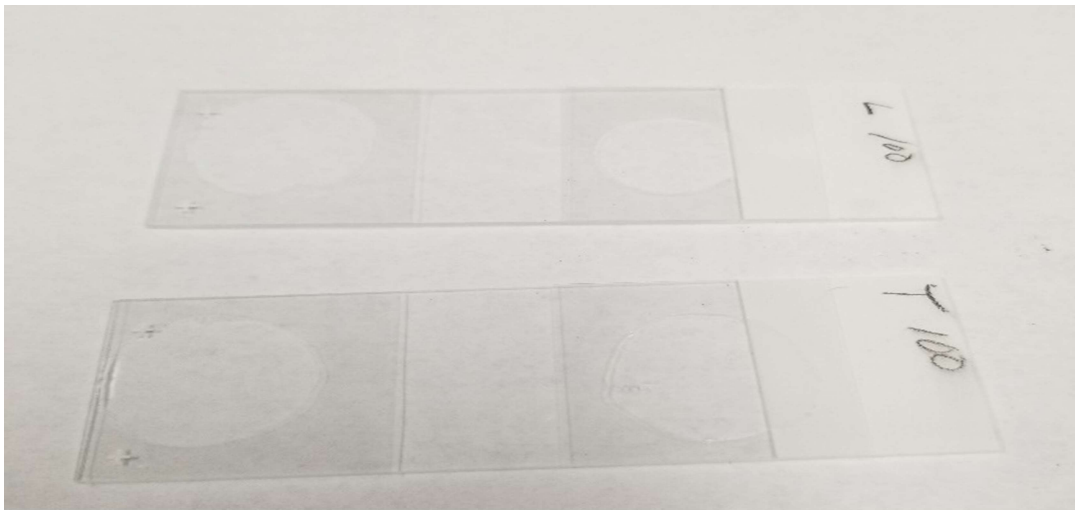

Figure 3.4. Early attempts at creating the gelation chamber

After the samples were put into the gelation chamber, the chambers were placed in an incubator at 37^0C, for 2 hours to polymerize. Figure 3.5, Figure 3.6, and Figure 3.7 show the sample once the polymerization was complete. The extra gel around the sample had to be removed, and the gelled sample itself removed from the microscope slide in order to perform the digestion and expansion steps.

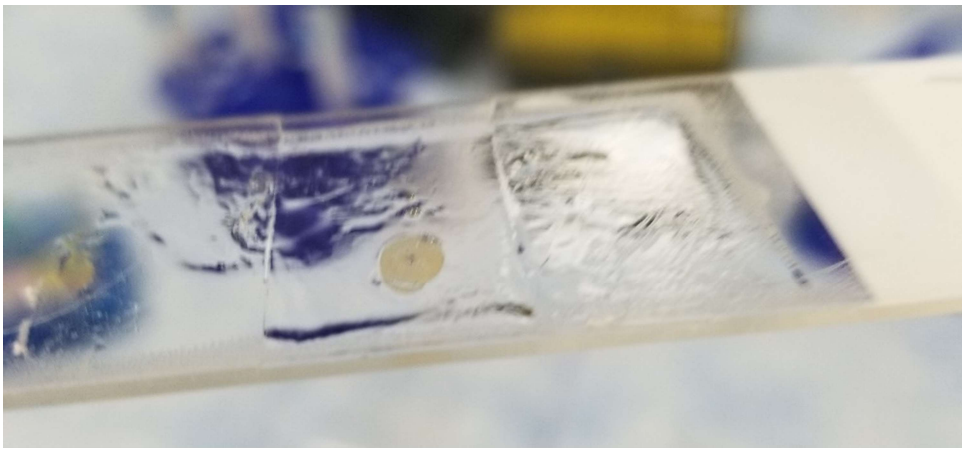

Figure 3.5 Gelled sample after polymerization at 37^0C.

Figure 3.7. Gelled removed from the gelation chamber.

Figure 3.6 Gelled sample after the surrounding gel was removed.

After polymerization the tissue in gels had to be digested for the sample to be able to expand isotropically. The gels were digested overnight in a Proteinase K solution. Figure 3.8 and Figure 3.9 show the samples before and after the overnight digestion. As evidenced in Figure 3.9, once the samples were digested, the gels expanded slightly and became clear. Figure 3.9 also shows the samples prior to the expansion. Figure 3.9 and Figure 3.10 show a before and after size comparison of the samples were soaked in deionized water.

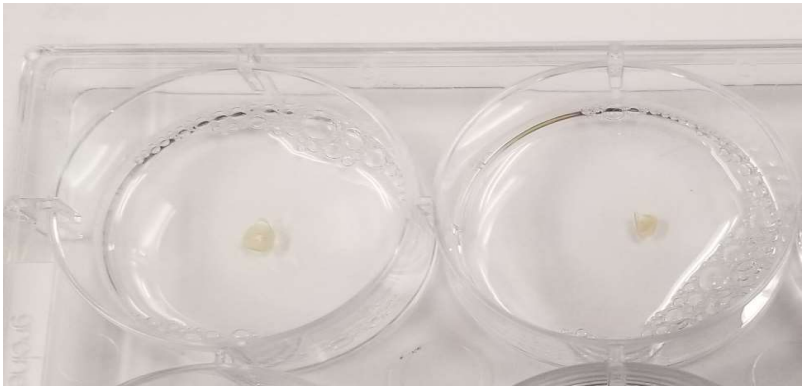

Figure 3.8. Gelled samples in digestion buffer.

For comparison, the images in Figure 3.9 and 3.10 were enlarged and scaled so that the wells in the before and after images were the same size. An oval was drawn around the samples, as close to the edges of the sample as possible. Height and width measurements were taken for each sample and the area was calculated. Sample A was calculated to have a pre expansion height of 0.76 inches, a width of 0.84 inches, and an area of 0.501 inches. Sample B was calculated to have a pre expansion height of 1 inch, width of 0.79 inches, and area of 0.621 inches. Post expansion, sample A was calculated to have a height of 1.72 inches, width of 1.91 inches, and an area of 2.580 inches. Post expansion sample B was calculated to have a height of 2.77 inches, a width of 2.18 inches, and an area of 2.580 inches. Sample A exhibited a 5.69X increase in size, and sample B exhibited a 7.60X increase in size.

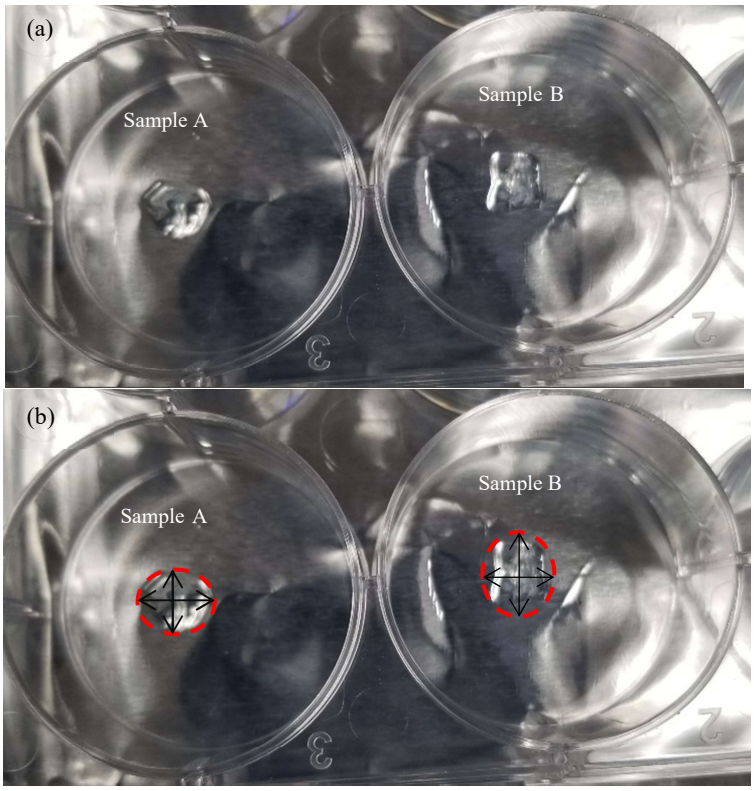

Figure 3.9 (a) Gelled samples after overnight digestion. (b) Measurement diagram of samples pre expansion.

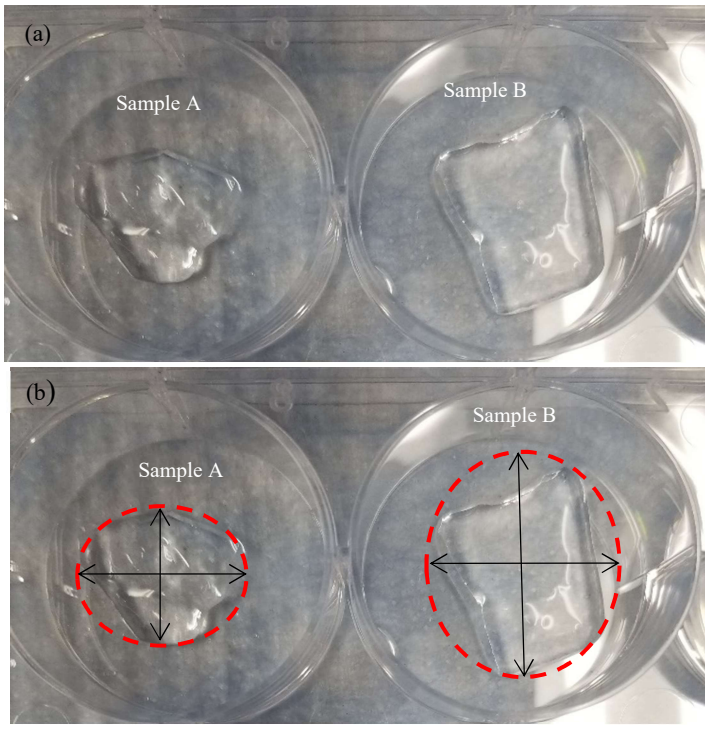

Figure 3.10. (a) Gelled samples after expansion. (b) Measurement diagram of expanded samples.

Once expanded the gels proved to be extremely delicate. Expanding the samples in a 6-well plate caused difficulty in moving the samples to a slide or imaging gasket to be imaged. One of the later adjustments made to the experiment was to transfer the unexpanded samples to imaging gaskets after the digestion step. The gaskets were then placed in Petri dishes, and the deionized

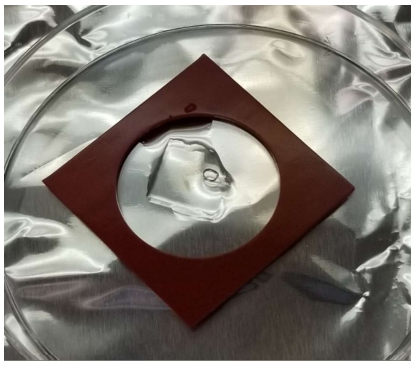

Figure 3.11. Expanded sample inside gasket.

water was added to expand the sample. Figure 3.11 shows the configuration of the sample, gasket, and Petri dish after the expansion process.

3.1.3 Expansion Images

Images of the prepared samples were taken before and after the expansion process. One of the most challenging aspects of the process is making sure the sample is placed flat inside the gelation chamber, and that it stays flat. This was a difficulty that was not overcome during this experiment. Also, the expanded samples are transparent, and the fluorescent labels within the sample are separated, so there is a large degree of reduction in signal collected during the imaging process. The intensity of the laser and sometimes the pinhole diameter needed to be increased to be able to obtain enough signal. The de-crowding of the fluorescent labels isotropically also reduced the relative area of the structure in the sample being imaged. These limitations reduced the amount of information represented by 2-dimensional samples to nearly nothing. The 2-demensional images of the pre-expanded rat hippocampal tissue can be found in section 3.1.1, above. The best analysis for the expanded tissue was to obtain 3-dimensional z-stack images and projections. Figure 3.12 through Figure 3.17 below show the pre and post expansion images of the hippocampal tissue, using the 20X and 40X water immersion objectives. The images below are screenshots of the z-stack projections at multiple angles. The comparison of pre and post expansion images at 20X and 40X magnification show that the structures imaged within the samples are physically larger in the post-expansion samples than the pre-expansion samples. Figure 3.12 shows screenshots of the pre-expansion z-stack projections at 20X and 40X. Figure 3.13 shows screenshots of the post-expansion z-stack projections at 20X and 40X. The scale bars for the 20X projections are 20 um, and the scalebars for the 40X projections are 50 um.

Figure 3.14 and Figure 3.15 are also screenshots of the z-stack projections. These figures show side-by-side comparisons of the pre-expansion and post expansion images at 20X and 40X magnification. These images were taken in the same areas of the same samples pre and post

expansion. It is shown in these images that the post expansion samples have been physical magnified, as the structures appear much larger in the post-expansion images. It is clear that the GFAP (red, astrocytes) labeling held its structure and fluorescence well during the process, but due to the decrowding and subsequent decreased concentration of the NeuN (green, neurons) labeling, the neuronal structures are more difficult to discern especially in Figure 3.15b, the 40X magnification post-expansion image.

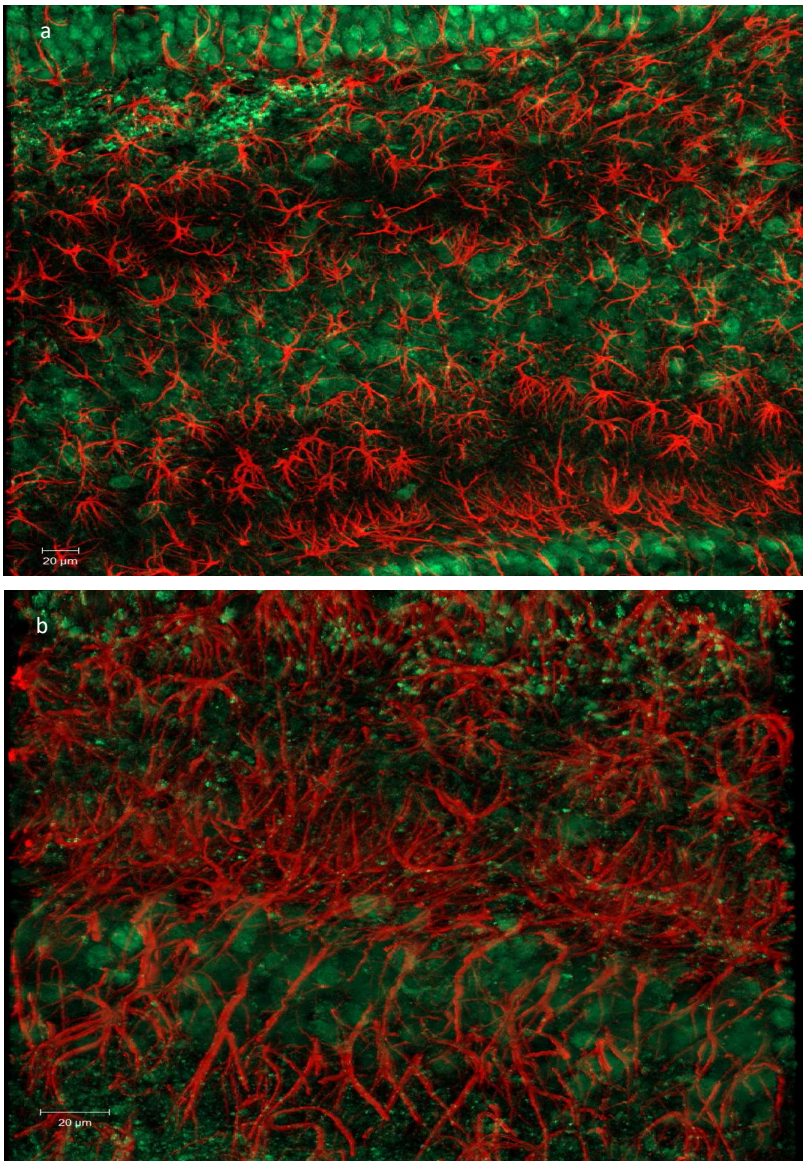

Figure 3.12. Screen shots of z-stack projections, pre expansion. (a) screenshot of image at 20X magnification (b) screen shot of image at 40X magnification.

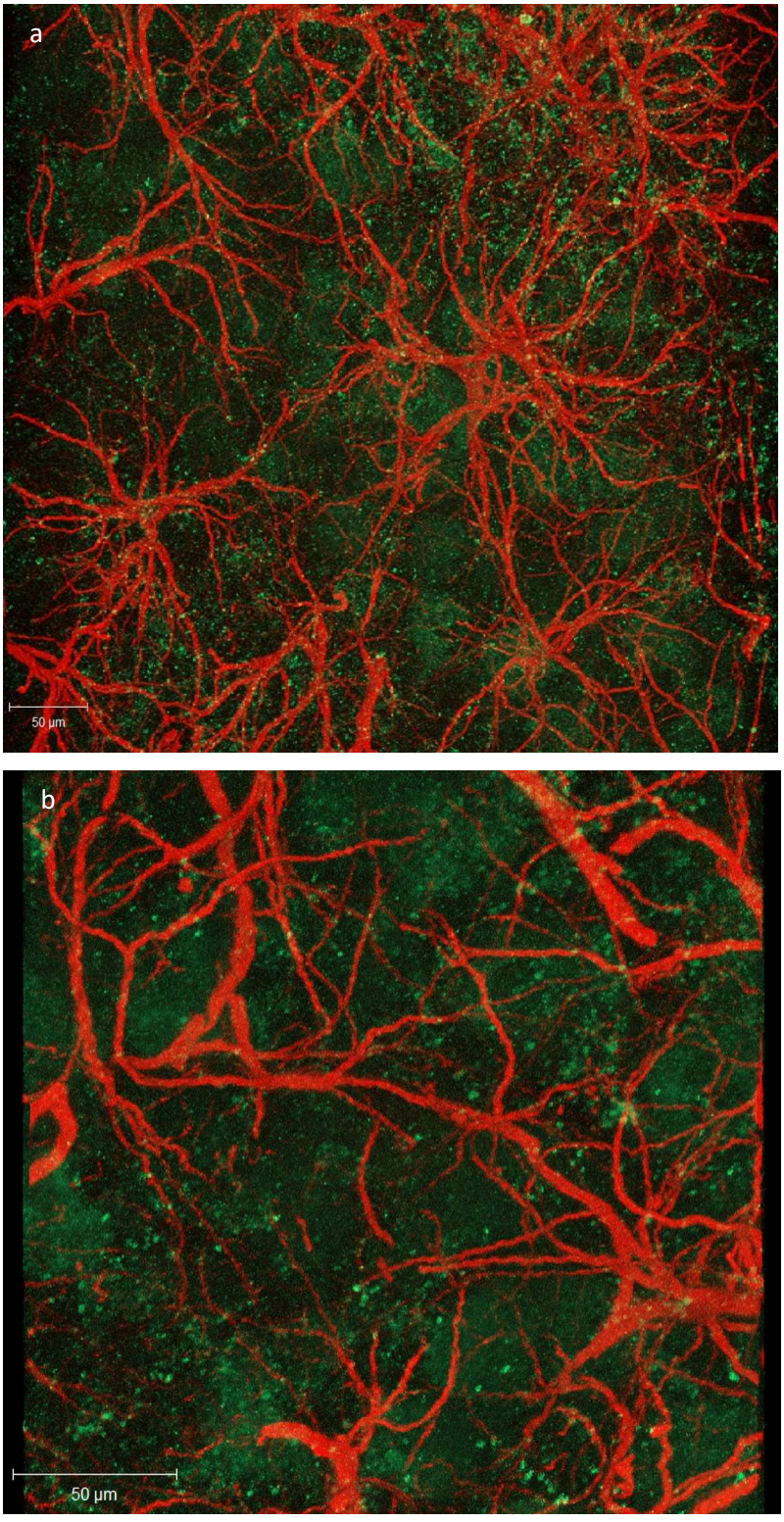

Figure 3.13. Screen shots of z-stack projections, post expansion. (a) screenshot of image at 20X magnification (b) screen shot of image at 40X magnification.

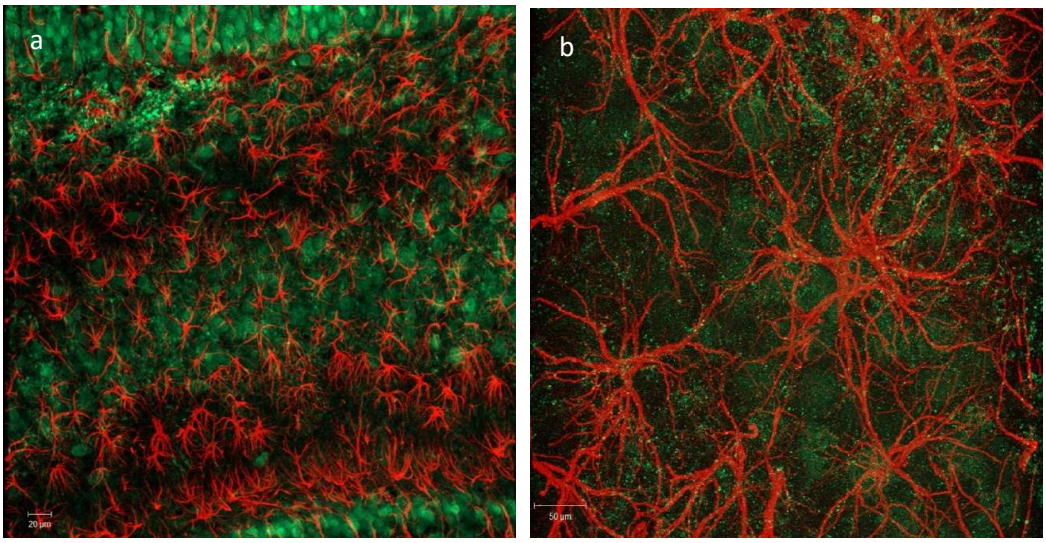

Figure 3.15. Side-by-side comparison of pre and post expansion images at 20X. (a) z-stack projection of pre expansion tissue at 20X, scale par: 20 um (b) z-stack projection of post expansion tissue at 20X, scale bar: 50 um

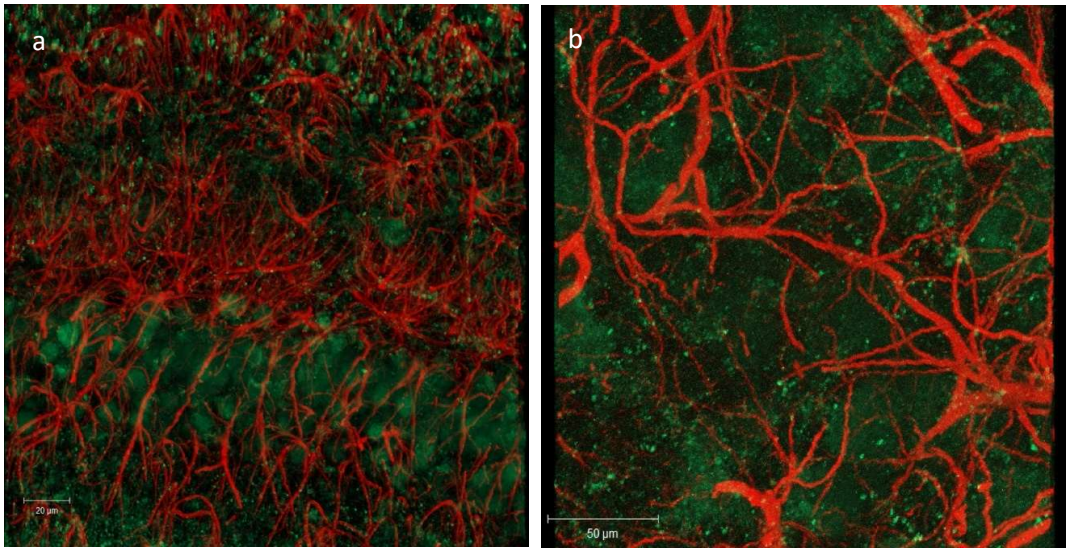

Figure 3.14. Side-by-side comparison of pre and post expansion images at 40X. (a) z-stack projection of pre expansion tissue at 40X, scale par: 20 um (b) z-stack projection of post expansion tissue at 40X, scale bar: 50 um

Figure 3.16 and Figure 3.17 show the side-view screenshots of the z-stack projections. These images are representative of the thickness of the z-stack images. When the z-stacks were taken, the first and last image setting were assigned to the locations at the top and bottom of the

sample. During imaging the stage height was adjusted until the visible structures were no longer discernable, and the first and last images were assigned at those locations. In Figures 3.16 and 3.17, the pre and post expansion side-view of the projections, the pre expansion z-stack size was 40.19 um and 43.21 um respectively. The pre-expansion 20X images have an X/Y/Z resolution of 450 um x 450 um x 40.19 um, an optical slice thickness of 3.1 um, and a stack size of 14; and the 40X images have an X/Y/Z resolution of 225.3 um x 225.3 um x 43.21 um, a optical slice thickness of 2.3, and a stack size of 39. The sample had a thickness of 40 um, therefore these samples are good representations of the actual thickness of the sample. The small variation in the size of the z-stack image versus the "actual" thickness can be accounted for by variations in cutting, or possibly the sample not lying flat while imaging. The post-expansion z-stack thicknesses are 191.66 um for the 20X magnification, and 200.77 um for the 40X magnification. The post-expansion images for the 20X objective have an X/Y/Z resolution of 449.5 um x 449.5 um x 43.21 um, an optical slice thickness of 3.1 um, and a stack size of 61; and the images for the 40X objective have an X/Y/Z resolution of 225.3 um x 225.3 um x 200.77 um, an optical slice thickness of 2.7 um, and a stack

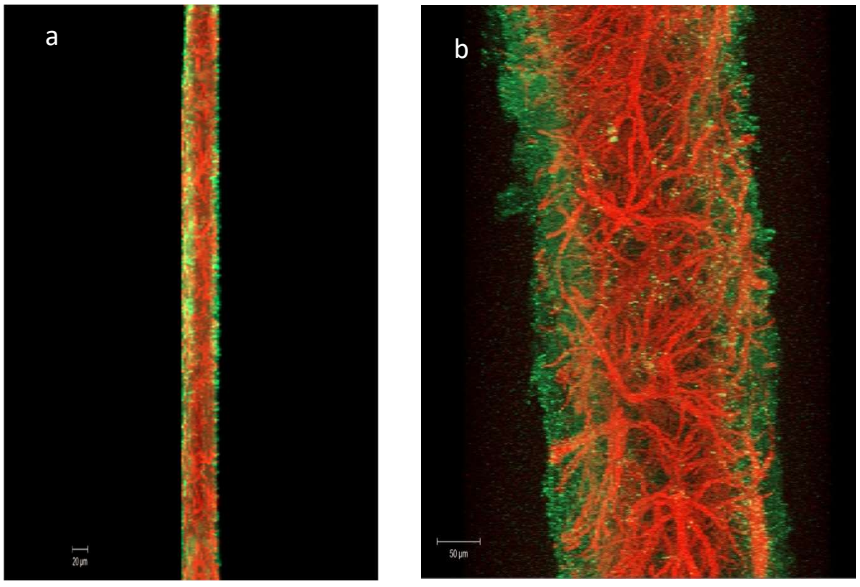

Figure 3.16. Side-by-side comparison of pre and post expansion z-stack projection thicknesses at 20X. (a) z-stack projection of pre expansion tissue at 20X, scale par: 20 um (b) z-stack projection of post expansion tissue at 20X, scale bar: 50 um

size of 74. The increase in the z-plane thickness shows an approximately 4.7X increase in the physical thickness of both samples.

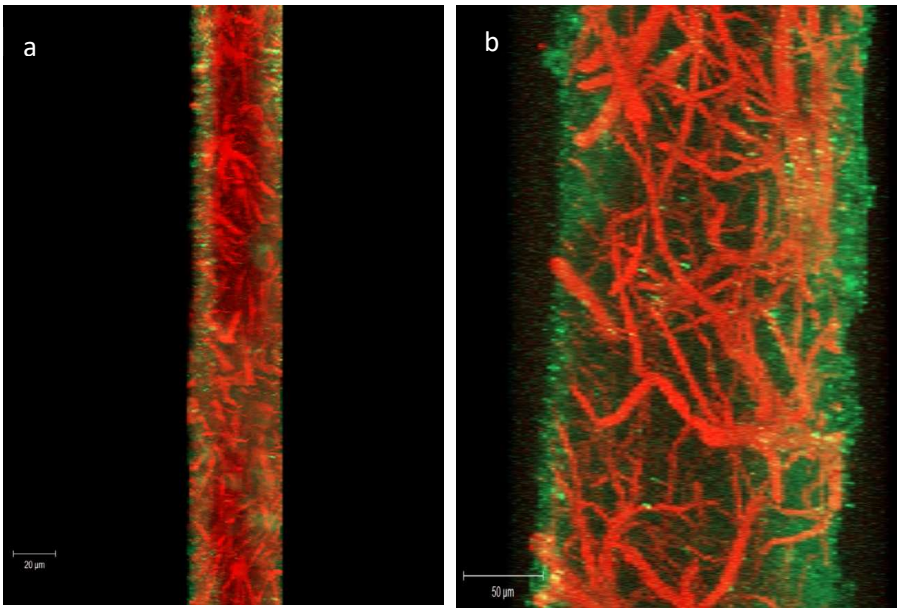

Figure 3.17. Side-by-side comparison of pre and post expansion z-stack projection thicknesses at 40X. (a) z-stack projection of pre expansion tissue at 40X, scale par: 20 um (total thickness: 43.21 um) (b) z-stack projection of post expansion tissue at 40X, scale bar: 50 um (z-stack thickness: 200.77 um)

3.2 EXAMINE THE ABILITY OF PROTEIN RETENTION EXPANSION MICROSCOPY TO EVALUATE CELLULAR JUNCTIONS IN CARDIAC TISSUE

The results of the experimentation with heart tissue were unfortunately negative. Several difficulties were faced when attempting to expand the cardiac tissue and will be further discussed in Section 5. The primary failure of this process was the inconsistent expansion of the tissue. Staining, gel embedding, and digesting the tissue were all successful in the process, but when the tissue expanded, some areas of tissue seemed to fully expand, as there were visible cell nuclei with vast amounts of space in between them, but other areas of tissue seem to barely expand at all. Some of these areas seemed to be clustered near what may have been vasculature within the tissue. When imaging in the 488 (green) channel, there is the possibility of vascular structures within the tissue

autofluoresing and showing structure other than what is being labeled. In Figure 3.18 below the green structures are the phalloidin 488 labeled actin filaments in the cytoskeleton. In Figure 3.19, there appear to be no actin filaments. Since the vasculature can autofluoresce in the 488 channel , the green structures in Figure 3.19 are thought to be vascular structures within the tissue. The results can be seen in Figure 3.18 and Figure 3.19 below. Figure 3.18 shows screenshots of the 3D z-stack

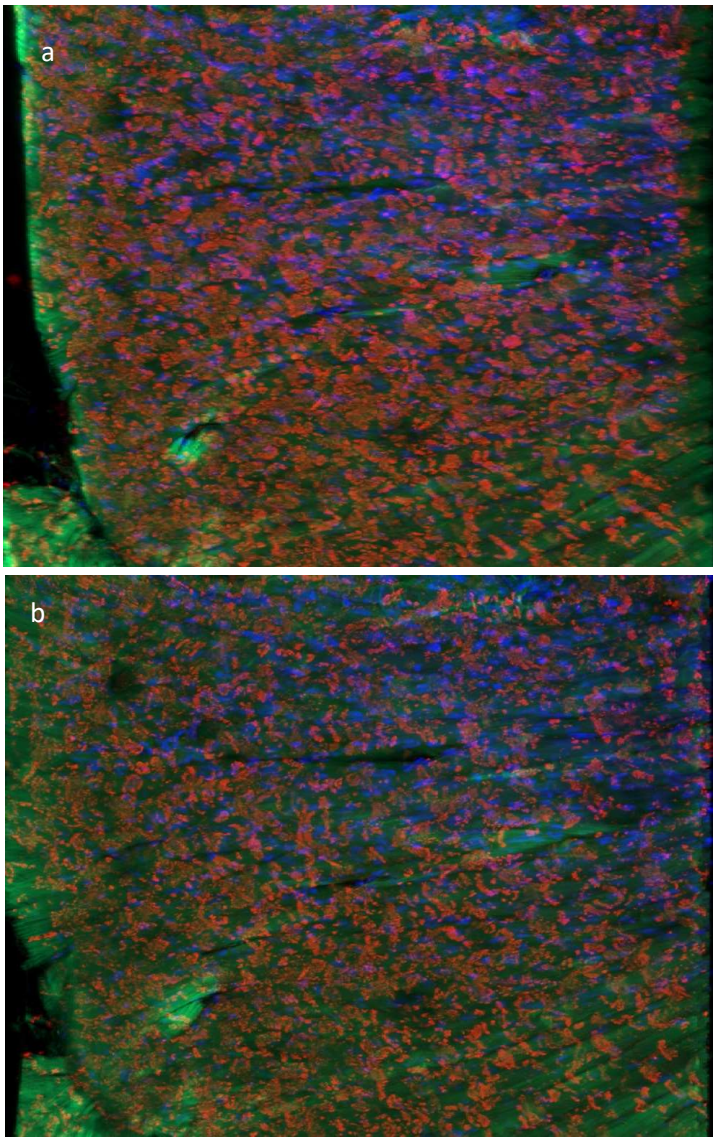

Figure 3.18. (a and b) Screenshots of different orientations of the z-stack projection of mouse cardiac tissue prior to expansion, showing the cytoskeletal actin filaments labeled by Phalloidin (green), the connexin proteins in the gap junctions (red), and the cell nuclei labeled by DAPI (blue).

projection of the fluorescently stained cardiac tissue before applying the ProExM technique; with an X/Y/Z resolution of 449.5 um x 449.5 um x 90.4 um, an optical slice thickness of 3.1 um, and an optical slice count of 30.

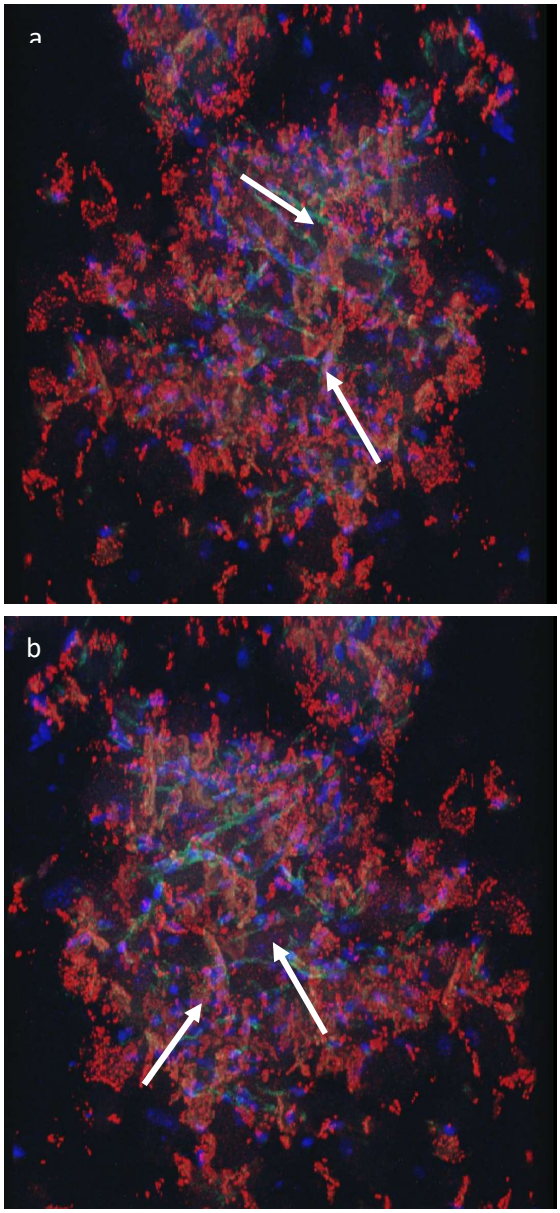

Figure 3.19. (a and b) Screenshots of different orientations of the z-stack projection of mouse cardiac tissue post-expansion.

Figure 3.19 shows screenshots of the same tissue sample, post expansion; with an X/Y/Z resolution of 450.0 um x 450.0 um x 174.5 um, an optical slice thickness of 3.1 um, and an optical

slice count of 57. Both z-stacks were taken with the 20X water immersion objective. These images show a complete disorientation of the tissue. The connexin proteins in the gap junctions (red) and the cell nuclei (blue) are visible but indicate no cellular orientation. Indicate by the white arrows.

3.3 DESIGN OF A NEW GELATION CHAMBER

With the aid of the School of Medicine machine shop, Mike Gore and Matthew Efird, a new gelation chamber layout was designed. This mechanism acts as fixture for use with a microscope slide, and slide covers to act as spacers and a lid. The fixture is a block of polymer which has sections bored out to hold a 1inch by 3 inches by 0.0364 inches, standard microscope slide. There are grooves placed 22 mm apart that are 0.160 mm deep into the polymer. These grooves act as channels to hold the microscope slide cover to make the spacers in the chamber. Finally, there is a groove bored out in the center of the slide seat so that the chamber lid can be set in place, and the chamber can be filled from the side. Figure 3.20 shows the gelation chamber fixture schematic, as designed by Matthew Efird.

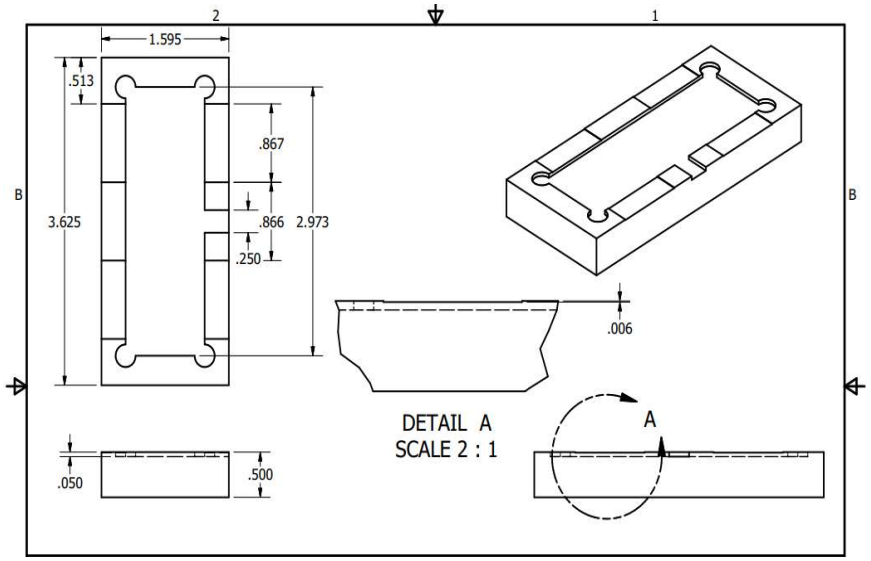

Figure 3.20. Gelation chamber prototype design showing measurements for accommodating a 1in x 3in x 1mm microscope slide, and two No 1.5 slide coverslips.

Figure 3.21 and Figure 3.22 show the new gelation chamber prototype in use with biological samples. The structure and stability of the fixture allows for easier creation of the chamber and morere uniform sample processing.

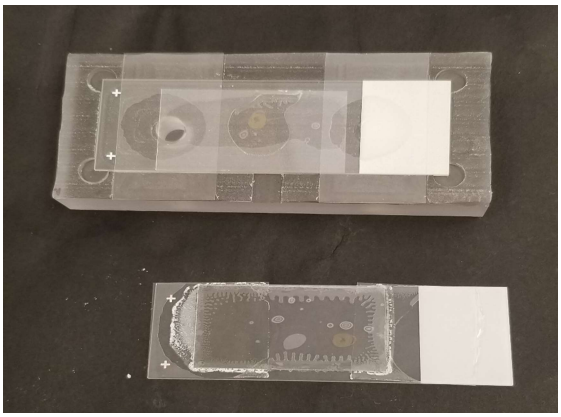

Figure 3.22. Comparison of traditionally constructed gelation chamber (bottom) and new gelation chamber prototype with samples.

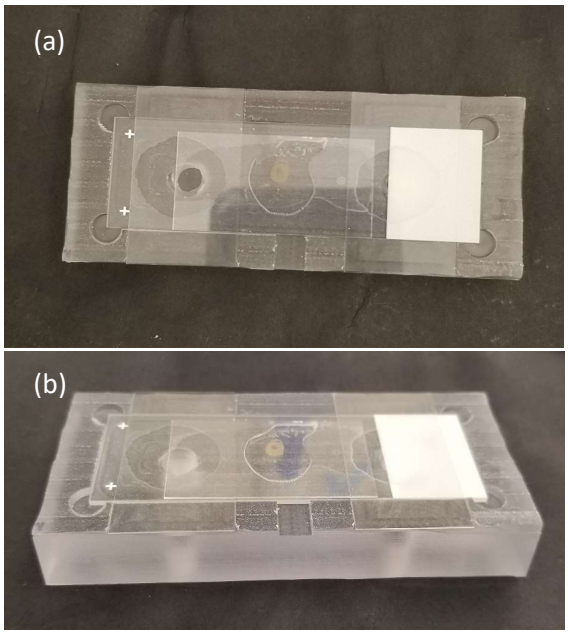

Figure 3.21. (a) Top view of new gelation chamber with sample, (b) side view of new gelation chamber with sample.

Chapter 4. DISCUSSION

4.1 DEVELOPMENT OF A PROTOCOL FOR USE IN THE IRF

It is clear from the results presented in Section 3 that the Protein Retention Expansion Microscopy technique is successful in producing at least a 4-fold increase in physical size of a prepared sample, and thus facilitates the imaging of microscopic structures. Throughout the course of this experiment, many difficulties were faced.

The labeling of the samples is a challenge that is encountered during any sample preparation. The important factors to address are identification of the correct labels for imaging the desired structures, properly permeabilizing the sample so that the labels can bind to their targets without destroying the sample, and using the correct concentration of label to dilutant to maximize the areas of interest that are labeled without wasting expensive antibodies. The staining procedure for the brain tissue called for 0.4% Triton-X 100 to permeabilize the tissue in nearly every step. This proved to be too high a concentration, and some of areas of the tissue were damaged in the process. In future experiments, it may be beneficial to use a lower concentration of Triton for the brain tissue.

Coupling sample staining with the ProExM procedure makes the choice of label and concentration more important. Since the process pulls the labels apart from each other, there can be a severe reduction in fluorescence concentration. This is most evident with the green neuron labels in the 40X magnification, post-expansion images in Section 3. The expansion procedure does increase the distance between the labels in the sample, but the extreme reduction in fluorescence was not seen in the GFAP labeled astrocytes. Since the GFAP and NeuN antibodies are comparable in size (50 kDA and 48 kDA respectively (Cell Signaling Tecnhnolgy, 2020)

(Millipore Sigma , 2020)), and both the AlexaFluor 546 and 488 are complete IgG antibodies, the size of the labels should not play a factor in the permeation, so it may be that the NeuN and AlexaFluor 488 may need more time to fully permeate the tissue. Also, most of the labeling in the green (488) channel is seen on the outside of the samples. This may be because the antibodies did not fully penetrate the tissue, but it also may be a limitation of the signal wavelength. Short wavelengths do not penetrate as deep into a sample as longer wavelengths. This often results in shorter wavelength signal not being detected in the middle of thick samples. The red channel has a wavelength of 546 nm, whereas the green channel has a wavelength of 488. The farther into a sample, the further the light has to travel, so light emitted from deep into the sample would not travel as far as the light emitted from the more shallow portions (Jerome & Price, 2018). Light emitted from deep into the sample in the 488 channel would also travel a shorter distance than light emitted from deep in the sample in the 546 channel. Possible future studies should include increasing the concentration of the NeuN and AlexaFluor 488 labels, and/or increasing the amount of time the samples are incubate in those labels. This may allow more attachment of the labels to the structures, and possibly increase the amount of fluorescence that can be detected post-expansion. Future studies may also include the use of a secondary label with a longer wavelength, such as a far-red label, with a 590 – 600 nm wavelength to examine whether or not those deep sample labels can be imaged.

During the process of gelling the samples to expand it is absolutely crucial to ensure that the chemicals used for the gelling solution are fresh and good, that the chemicals are kept cold, and that ratios of the chemicals in the solution are correct for the type and size of sample that is being prepared. This process is extremely temperature dependent; all chemical components must be kept cold to avoid premature setting of the gel. To accomplish this, the gelling solution components must be kept on ice or in a cold block. The mixing of the solution must also be performed with the chemicals as cold as possible. The process of mixing the gelling solution can also be done on ice, or inside a cold room.

The freshness and ratio of the chemicals is vital to proper gelled sample creation. Throughout this experiment it was found that the TEMED activator solution should be made fresh before mixing it into the gelling solution. The TEMED is used in the gelling solution to activate the ammonium persulfate (APS) and acrylamide to solidify into the gel, if it is too old the gel will completely polymerize. Also, the ratios of the chemicals are crucial. The APS and the monomer solution are the basis of the gel. The APS and the acrylamide within the monomer solution create the base gel structure, while the N,N'-Methylenebisacrylamide provides the crosslinking within the gel that allows the isotropic expansion. The rest of the monomer solution is primarily composed of PBS and sodium chloride solution. These components create a dehydrated environment in the gel. This allows the gel to absorb the water during the expansion process. One key component to the gelation solution is 4HT, which acts as a polymerization inhibitor. It may seem counterintuitive to add an inhibitor to a solution created to polymerize and create a gel, but in the process of expansion microscopy it is essential. The gelation solution must not only encase the sample, but it must permeate the sample so that once the sample is digested the gel is uniform in structure to allow for isotropic expansion. The sample must incubate in the gelation solution for 30 to 60 minutes prior to polymerization. This allows the solution to soak into the sample. The 4HT inhibitor prevents the gel from setting while the sample is incubating. Samples of tissue that are greater than 200 um in thickness, or samples that are specifically dense (i.e. cardiac tissue) required a longer incubation in the gelation solution than thin samples. This also requires the gelation solution to resist polymerization longer. In these instances, the amount of 4HT is increased to allow for the longer incubation.

Other difficulties that come with performing expansion microscopy is the delicacy and size of the expanded gels. Prior to expansion, it is very important to locate the area of interest. During the course of this experiment, it was found that the best way to do this was to remove the hippocampus before staining. Identifying and removing the area of interest after staining led to photobleaching of the labels, thus it was necessary to remove the area before staining. This also

yields a smaller sample to process. Smaller samples create small expanded gels. Once expanded, the gels are very delicate and are easily destroyed if handled. In the early attempts at this procedure, many samples were destroyed when attempting to relocate them from the vessel in which they were expanded to the microscope slide for viewing. It was found that when using a large, flat paintbrush the sample could be relocated, but only if the sample itself was small enough to fit on the paintbrush. Unfortunately, this method was also less than ideal, as the gels would often stick to the paintbrush and fall apart when they were being transferred to the slide. To solve this problem, it was found that the best way to expand the samples was to place the unexpanded sample in imaging gaskets, and the gaskets in a Petri dish, then adding the deionized water to the gasket inside the Petri dish. Examples of this method can be seen in Results Section 3.1.2.

This experiment has shown that expansion microscopy is a strong tool for the viewing of microscopic structures, but more can be examined in this technique. As stated before, future experiments should include increasing the concentration and/or the incubation time of the NeuN labeling. Another future analysis would be examining the colocalization of structures and molecules. Dr. Ana Pocivavsek of the University Of South Carolina School Of Medicine and her laboratory associates study the enzyme Kynurenine Aminotransferase II (KATII) in many neurological studies. KAT II is an enzyme that is located in astrocytes (Guidetti, 2007) (Wu, 2014); using Dr. Pocivavsek's KAT II antibody along with the GFAP labels rat hippocampal tissue can be examined for the colocalization of the KAT II in the astrocytes.

4.2 Examine the ability of Protein Retention Expansion Microscopy to evaluate cellular junctions in cardiac tissue

There were many difficulties with using expansion microscopy to analyze cardiac tissue. First, a new staining protocol had to be developed. One specific downfall to expansion microscopy in general is the reduction of detectable fluoresce. The IRF's standard procedure for staining cardiac tissue was found to give the antibodies insufficient time to anchor enough label to the tissue to

survive the process. Using a variation on staining procedures that are used when X-Clarity is in use, the times that the primary and secondary antibodies, as well as the other fluorescent stains were allowed to incubate were increased substantially. This increase allowed more labels to attach to more areas on the surface, and throughout the thickness of the tissue. The introduction of more labels gave a greater chance of obtaining solid post-expansion images; unfortunately, this method did not solve all of the problems. Aside from increasing the amount of time the tissue was exposed to the labels, the amount of time that the tissue was treated with Triton-X 100 was increased to increase the permeabilization of the tissue.

When examining the expanded heart tissue, little to no signal was detected when imaging in the green (488) channel. Even the visible evaluation showed almost no structures in the tissue. Collagen and elastin have been known to autofluoresce in the green channel so it is possible that any structures that were discernable were just the vascular structures autofluorescing in green. After further literature review it has been found that phalloidin labeling is incompatible with expansion microscopy. Phalloidin is considered a "small labeling molecule (Wen, 2020)," and it has been found that such molecules "can be difficult to link to the gel matrix and are washed out of the sample during the expansion process (Wen, 2020)." To overcome this problem Wen, et. al. developed a method of "antibody-free labeling" that employs trivalent anchoring (Wen, 2020). To further examine the efficacy of expansion microscopy with cardiac tissue, a different method of labeling should be employed to ensure the retention of cellular structure and orientation.

It has been shown that cardiac tissue does not expand uniformly when used with the ProExM procedure. Part of this may be due to the high-density areas of collagen and elastin within the tissue. This may be one reason that the areas around what may be autofluorescing vasculature showed dense (relative to other areas of expanded tissue) cellular nuclei and connexin-43 labeled areas. Dr. Izzy Jayasinghe of the University of Leeds has also been working on the use of protein retention expansion microscopy in the examination of cardiac tissue. In correspondence, she relayed that the main obstacle that her group had experienced was the large amounts of collagen

that needed to be digested, and recommended using a longer digestion time; but the specific digestion time needed to be tailored to the areas of interest and the labels being used. Her group is currently in the process of compiling a protocol on the use of ProExM with cardiac tissue. With this advice, it was decided to treat the heart tissue samples as "thick tissues," and use the thick tissue variations outlined in the Asano protocol (Asano, 2018). Even with the extended staining, the thick tissue variation, and a 3-day digestion process, the experiment was still unsuccessful. Further study, including a full review of Dr. Jayasinghe's protocol is needed to perform protein retention expansion microscopy when examining intercalated discs, and using a phalloidin stain as part of the cellular spatial examination.

4.3 Design of a New Gelation Chamber

The design of the new gelation chamber required several draft ideas, and much collaboration. Several iterations of the design were discussed, but finally it was decided that the best way to ensure a flat and even gel was to utilize the flat even surface of a microscope slide and cover slips. With the expansion of the gels, any ridges or bumps are magnified 4-fold, so boring out a channel for the gel would not guarantee a flat and even surface. The chamber fixture was created to give a stable base and keep all the aspects in place when creating the gels. The fixture also allows for a uniform creation of gels to ensure repeatability. One of the difficulties with polymerizing the gels is transferring them from the preparation area to the incubator for polymerization. The new fixture provides a strong and stable base that locks in the components of the chamber and allows for more stable relocation during the polymerization process, but improvements can be made. The prototype chambers design specifications were created off of one microscope slide, so small differences in the manufacturing of the slides can cause problems if the slide is slightly larger than the channel. Relaxing the tolerance of the length and width of the slide channel by 0.05 inches may facilitate the use of the fixture and make up for manufacturing variations in the slides.

REFERENCES

Artur, C. W. (2018). Plasmonic nanoparticle-based expansion microscopy with surface-enhanced Raman and dark-field spetroscopic imaging. *Biomedical Optics Express, 9*(2), 603-615. doi:10.1364/BOE.9.000603

Asano, S. M. (2018). Expansion microscopy: Protocols for imaging proteins and RNA in cells and tissues. *Current Protocols in Cell Biology, 80*, e56. doi:10.1002/cpcb56

Bucur, O. Y. (2016). Physical expansion of tissue microarrays for high-resolution imagin of normal and cancer samples with conventional microscopy. *Proceedings of the 107th Annual Meeting of the American Association for Cancer Research. 76*, pp. 16-20. New Orleans, LA: Cancer Res.

Bucur, O. Z. (2018). Nanoscale Imaging of Kidney Glomeruli Using Expansion Pathology. *Fronteirs in Medicine, 5*, 322. doi:10.3389/fmed.2018.00322

Burgers, J. P.-G. (2019, Jan 6). Light-sheet fluroescent expansion microscopy: fast mapping of neural circuits at super resolution. *Neurophotonics*, 015005. doi:10.1117/1NPh.6.1.015005

C hang, J. C. (2017). Iterative Expansion Microscopy. *Nature Methods, 14*(6), 593-599. doi:10.1038/nmeht.4261

Cahoon, C. Y. (2017). Superresolution microscopy reveals the three-dimensional organization of the Drosophila synaptonemal complex. *Proceedings of the National Academy of Sciences of the United States of America. 114*, pp. E6857-E6866. Washigton, DC: National Academy of Sciences of the United States of America. doi:10.1073/pnas.1705623114

Cell Signaling Tecnhnolgy. (2020, July 19). *GFAP (D1F4Q) XP RAbbit mAb #12389*. Retrieved from Cell Signaling Technologies: https://www.cellsignal.com/products/primary-antibodies/gfap-d1f4q-xp-rabbit-mab/12389?site-search-type=Products

Chang, J. C. (2017, June). Iterative Expansion Microscopy. *Nature Methods, 14*(6), 593-599. doi:10.1038/nmeth.4261

Che n, F. T. (2015). Optical imaging. Expansion microscopy. *Science, 347*(6221), 543-548. doi:10.1126/science.1260088

Chen, F. T. (2015, January 30). Expansion Microscopy. *Science, 347*(6221), 543-548. doi:10.1126/science.1260088

Chen, F. W. (2016, August). Nanoscale imaging of RNA with expansion microscopy. *Nature Methods, 13*(8), 679-684. doi:10.1038/nmeth.3899

Choiznski, T. M. (2018). Volumetric Nanoscale Optical Imaging of Mouse and Human Kidney via Expansion Microscopy. *Scientific Reports, 8*(1), 10396. doi:10.1038/s41598-018-28694-2

Chozinski, T. H. (2016, June). Expansion Microscopy with Conventional Antibidies and Flourescent Proteins. *Nature Methods, 13*(6), 485-488. doi:10.1038/nmeth.3833

Crittenden, J. T. (216). Striosome-dendrom boquets highlight a unique striatonigral curcuit targeting dopamine-containing neurons. *Proceedings of the National Academy of Sciences of the United States of America, 113*(40), 11318-11323. doi:10.1073/pnas.1613337113

Delete. (2018, August). Expansion Microscopy: Protocols for Imaging Proteins and RNA in Cells and Tissues. *Current Protocols in Cell Biology, 80*(1). doi:10.1002/cpcb.56

Deshpande, T. L. (2017, Nov). Subsellular Reorganization and Altered Phosphorylation of Astrocytic Gap Junction Protein Connexin43 in Human and Experimental Lobe Epilepsy. *Glia*, 10891820. doi:10.1002/glia.23196

Enger, P. F. (2016, Sept). Super-resolution microscopy writ large. *Nature Biotechnology, 34*(9), 928-930. doi:10.1038/nbt.3669

Feng, H. W. (2018). Super-Resolution FLourescence Microscopy for Cell Imaging. *Advances in Experimental Medicine and Biology*(1068), 59-71. doi:10.1007/978-981-13-0502-3_6

Freifeld, L. O.-A. (2017, November 21). Expansion microscopy of zebrafish for neuroscience and developmental biology studies. *PNAS*, E10799-E10808. doi:10.1073/pnas.1706281114

Ga o, M. M. (2018, May 22). Expansion Stimulated Emission Depletion Microscopt. *ACS Nano, 12*(5), 4178-4185. doi:10.1021/acsnano.8b00776

Galbraith, C. G. (2011, may 15). Super-resolution microscopy at a glance. *Journal of Cell Scuence, 124*(10), 1607-1611. doi:10.1242/jcs.080085

Gambarotto, D. Z.-C. (2019). Imaging cellular ultrastructures using expansion microscopy. *Nature Methods, 16*(1), 71-74. doi:10.1038/s41592-018-0238-1

Gao, R. A. (2017). Q&A: Expansion Microscopy. *BMC Biology, 15*(50), 1-9. doi:10.1186/s12915-017-0393-3

Grafe, M. B. (2019). Supramolecular Structures of the Dictyostelium Lamin NE81. *Cells, 8*(2), 162. doi:10.3390/cells8020162

Guidetti, P. H.-F. (2007, Jan). Astrocytic location of kynurenine aminotransferase II in the rat brain visualized by immunohistochemistry. *Glia, 55*(1), 78-92.

Hafner, A. D. (2019, May 17). Local Protein Synthesis is a Ubituitous Feature of Neuronal Pre- and Postsynaptic Compartments. *Science, 364*, 6441. doi:10.1126/science.aau3644

Halpern, A. A. (2017). Hybrid Structured Illumination Expansion Microscopy Reveals Microbial Cytoskeleton Organization. *ACS Nano, 11*(12), 12677-12686. doi:10.1021/acsnano.7b07200

Jerome, W. G., & Price, R. L. (2018). *Basic Confocal Microscopy, Second Edition.* Cham, Switzerland: Springer Nature Switzerland AG.

Jiang, N. K. (2018). Superresolution of Dorsophila tissues using expansion microscopy. *Molecular biology of the cell, 29*(12), 14131421. doi:10.1091/mbc.E17-10-0583

Kao, P. N. (2019). Transctiptional Activation of Arabidopsis Zygotes is Required fro Initial Cell Divisions. *Scientific Reports, 9*(1), 17159. doi:10.1038/s41598-019-53704-2

Karagiannis, E. a. (2018). Expansion microscopy: development and neuroscience applications. *Current Opinion in Neurobiology*(50), 56-63. doi:10.1016/j.conb.2017.12.012

Kaverina, N. E. (2019, Sep). Dual lineage tracing shows that glomerular parietal epithelial cells can transdifferentiate toward the adult podocyte fate. *Kidney International, 96*(3), 597-611. doi:10.1016/j.kint.2019.03.014

Kim, D. K. (2019, May 15). Amplified Expansion Stimulated Emission Depletion Microscopy. *Chembiochem, 20*(10), 1260-1265. doi:10.1002/cbic.201800775

Klimas, A. B. (2019). Nanoscopic imaging of human tussue sections via physical and isotropic expansion. *J.Vis Exp, 151*, e60195. doi:10.3791/60195

Kunz, T. G. (2019). Detection of Chlamydia developmental forms and secreted effectors by expansion microscopy. *Frontiers in cellular and infection microbiology*(9), 276. doi:10.3389/fcimb.2019.00276

Lee, K. V. (2019, eb 6). Functional synaptic architecture of callosal inputs in mouse primary visual cortex. *Neuron, 101*(3), 421-428. doi:10.1016/j.neuron.25018.12.005

Li, R. C. (2018, Sep 27). Expansion Enhanced Nanoscopy. *Nanoscale, 10*(37), 17552-17556. doi:10.1039/c8nr04267e

Lim, Y. S. (2019). Mechanically resolved imaging of bacteria using expansion microscopy. *PLoS biology, 17*(10), e3000268. doi:10.1371/journal.pbio.3000268

Menon, K. K. (2019). Interations between Dpr11 and DIP-y control selection of amacrine neurons in Drosophil color vision circuits. *eLife, 8*, e48935. doi:10.7554/eLife.48935

Millipore Sigma . (2020, July 19). *Anti-NeuN Antibody, clone A60*. Retrieved from Millipore Sigma: https://www.emdmillipore.com/US/en/product/Anti-NeuN-Antibody-clone-A60,MM_NF-MAB377

Min, K. C. (2019, Jul 19). Multiplexed Expansion Microscopy of the Brain Through FLourophore Screening. *Methods*(18), S1046-2023. doi:10.1016/j.ymeht.2019.01.017

Mosca, T. L. (2017). Presynaptic LRP4 promotes symanpse number and function of excitatory CNS neurons. *eLife*(6), e27347. doi:10.7554/eLife.27347

Nielsen, M. A.-R. (2012). Gap Junctions. *Compr Physiol, 2*(3), 1981-2035. doi:10.1002/cphy.c110051

Pratten, B. K. (2014). Structure and Function of Gap Junction Proteins: role of gap juction proteins in embryonic heart development. *Internation Journal of Developmental Biology*(58), 649-6692. doi:10.1387/ijdb.140188dp

Rouhanifard, S. M. (2018). ClampFISH detects individual nucleic acid molecules using click chemistry-based amplification. *Nature biotechnology*, 4286. doi:10.1038/nbt.4286

Saka, S. W. (2019). Immuno-SABER enables highly multiplexed and amplified protein imaging in tissues. *Nature Biotechnology, 37*, 1080-1090. doi:10.1038/s41587-019-0207-y

Schermelleh, L. F. (2019, Jan). Super-resolution Microscopy Demystified. *Nature Cell Biology, 21*(1), 72-84. doi:10.1038/s41556-018-0251-8

Sheard, T. H. (2019). Three-dimensional and chemcial mapping of intracellular signaling nanodomains in health and disease with enhanced expantion microscopy. *ACS nano, 13*(2), 2143-2157. doi:10.1021/acsnano.8b08742

Tillberg, P. C. (2019). Protein-retention expansion microscopy of cells and tissues labeled using standard fluorescent proteins and antibodies. *Nature Biotechnology, 34*(9), 987-992. Retrieved from https://www-ncbi-nlm-nih-gov.pallas2.tcl.sc.edu/pmc/articles/PMC5068827/

Truckenbrodt, S. S. (2019). A practical guide to optimization expansion microscopy. *Nature Protocols, 14*, 832-863. doi:10.1038//s41596-018-0117-3

Truckenbrodt, S., Maidorn, M., Crzan, D., Wildgagen, H., Kabatas, S., & and Rixxoli, S. (2018, September). X10 Expansion Microscopy Enables 25-n Resolution on Conventional Microscopes. *EMBO Reports, 19*(9), e45836. doi:10.15252/embr.201845836

Ts ai, Y. T. (2019, Apr 9). Rapid High Resolution 3D imaging of Expanded Biological Specimens with Lattice Light Sheet Microscopy. *Methods, 18*, S1046-2023. doi:10.1016/i.ymeth.2019.04.006

Tsai, A. M. (2017, Nov). Nuclear Microenvironments Modulate Transcription From Low-Affinity Enhancers. *ELife, 6*, e28975. doi:10.7554/eLife.28975

Tsanov, N. S. (2016). smiFISH and FISH-quant - a felxible single RNA detection approach with super resolution capability. *Nucleic acids research, 44*(22), e165. doi:10.1093/nar/gkw784

Wang, G. M. (2018). Multiplexed imaging of high-densito libraries of RNAs with MERFISH and expansion microscopy. *Scientific reports, 8*(1), 4847. doi:10.1038/s41598-018-22297-7

Wang, I. L. (2016). Hedgegog signaling regulates gene expression in planarian glia. *eLIFE, 5*, e16996. doi:10.7554/eLife.16996

Wang, Y. Y. (2018). Combined expansion microscopy with structured illumination microscopy for analyzing protein complexes. *Nature Protocols, 13*, 1869-1895. doi:10.1038/s41596-018-0023-8

Wassie, A. Z. (2019, January). Expansion microscopy: principles and uses in biological research. *Nature Methods, 16*, 33-41. doi:10.1038/s41592-018-0219-4

Wen, G. V. (2020, Mar 26). Evaluation of Direct Grafting Strategies via Trivalent Anchoring for Enabling Lipid MEmbrane and Cytoskeleyon Staining in Expansion Microsopy. *ACS Nano*. doi:10.1021/acsnano.9b09259

Wu, H. O. (2014, Mar). Targeting kynurenine aminotransferase in psychiatric diseases: promising effectos of an orally active enzyme inhibitor. *Schizophrenia bulletin, 40*, Suppl 2:S152-158. doi:10.1093/schbul/sbt157

Xu, H. T. (2016, Sep 10). Molecular organization of mammalian meiotic chormosome axis revealed by expansion STORM microscopy. *Proced Natl Acad Sci USA, 116*(37), 18423-18428. doi:10.1073/pnas.1902440116

Zhang, Y. C.-d. (2016). Hybrid Microscopy: Enabling inexpensive high-performance imaging throught combined physical and optical magnifications. *Scientific Reports*(6), 22691. doi:10.1038/srep22691

Zhao, Y. B. (2017, August). Nanoscale imaning of clinical specimens using pathology-optimized expansion microscopy. *Nature Biotechnology, 35*(5), 757-764. doi:10.1038/nbt.3892

APPENDIX A: PROTOCOL FOR USE IN THE IRF

A.1. PROTOCOL

A.1.1 Materials and Equipment

A.1.1.1 Equipment

a. Vibratome

b. 24, 12, or 6 well plates*

c. Coverslips**

d. Microscope Slides

e. Microcentrifuge tubes

f. Paint brushes

g. Ice bath

h. Forceps

i. Imaging gaskets

j. Petri dishes

k. Microscope*

*Items varied per experiment and are defined in the printed protocol.

A.1.1.2 Chemicals, Fixation, and Sectioning

Table A.1 Chemicals used

Chemical	**Supplier**	**Cat no**
Phosphate Buffered Saline (PBS)	Sigma Aldrich	P3813-10PAK
Glycine	Sigma Aldrich	56-40-6
Triton-X 100	Sigma Aldrich	X100-100ML
Bovine Serum Albumin (BSA)	Jackson ImmunoResearch	001-000-162
Normal Donkey Serum (NDS)	Jackson ImmunoResearch	017-000-001
Tween 20	Sigma Aldrich	P9416-100ML
*Anti-Connexin 43, rabbit polyclonal antibody	Sigma Aldrich	C6219-2ML
*Invitrogen AlexaFluor 546, Donkey, anti-rabbit	ThermoFisher Scientific	A10040
*Invitrogen AlexaFluor 488 Phalloidin	ThermoFisher Scientific	A12379
*4',6-diamidino-2phenlindole,d (DAPI)	Molecular Probes	D1306
DABCO	Sigma Aldrich	290734
*anti-Neuronal Nuclei, mouse monoclonal antibody	EMD Millipore	MAB377
*anti-GFA, rabbit monoclonal antibody	Cell Signaling Technology	12389S
*anti-KATII, rabbit purified antibody	Covance	5499
*Invitrogen, AlexaFluor 405, goat anti-rabbit		
*Invitrogen AlexaFluor 488 mouse IgG, donkey	Molecular Probes	A21202
Acryloyl-X SE	ThermoFisher Scientific	A20770
Dimethyl Sulphoxide (DMSO)	Sigma Aldrich	D2650
N,N,N',N'-tetramethylethylene-diamine (TEMED)	BioRad	161-0800
Ammonium Persulfate (APS)	ThermoFisher Scientific	7727-54-0
4-hydroxy-TEMPO (4HT)	Aldrich	176141-5G
Sodium Acrylate	Aldrich	408220-25G
Acrylamide	Acros Organics	164835000
N,N'-Methylenebisacrylamide	Sigma Aldrich	M-7256
NaCl	Fisher Chemicals	S271-500
EDTA, disodium	BioRad	161-0729
Tris•CL	BioRad	161-0799
Proteinase K	ThermoFisher Scientific	EO0491
2-(N-morpholino)ethanesulfonic acid (MES)	Acros Organics	274140500

Tissues were fixed with the protocol of choice*, but for the purposes of this experiment; tissues will be fixed with 4% (w/v) paraformaldehyde (PFA) in PBs for 24 hours. Tissues can be sectioned using the method of choice, but for the purposes of this experiment; fixed samples were sectioned on the Leica VT12000 Vibratome. Mouse heart samples were sectioned transversely in 100 um thick sections. Mouse brain samples were sectioned coronally in 50 um thick sections. Tissues thicker than 200 um require alterations to the protocol. These alterations can be found in the 2018, Asano et al paper: Expansion Microscopy: Protocols for Imaging Proteins and RNA in Cells and Tissues, published in Current Protocols in Cell Biology. Tissues can be stained with the protocol of choice, but for the purposes of this experiment the following protocols were used.

A.1.2 Immunohistochemistry for mouse Brain Tissue

1. 15 min PBS/0.01M Glycine/0.1% Triton-X
2. 6 hour 5% Normal Serum/PBS
3. Overnight *Primary* (in 1% Normal Serum/PBS [1:100]) @ 4^0C

   Record Primary:_____
4. 4 X 15 min Rinse with 1% Normal Serum/PBS to remove any unbound antibodies
5. 1 hour 5% Normal Serum in PBS
6. **** COVER WITH FOIL *****
7. Overnight *Secondary* (in 1% Normal Serum/PBS [1:100]) @ 4^0C
8. Record Secondary: _____
9. 4 x 15 min Rinse with PBS to remove any unbound antibodies

A.1.3 Immunohistochemistry for mouse Heart Tissue

1. 5 hours PBS/0.01M Glycine/0.1% Triton-X
2. 1 hour 5% BSA/PBS
3. 1 hour 5% Normal Donkey Serum (in 1% BSA/PBS)

4. 48 hours *Primary* (1% BSA/PBS [1:100]) shaking gently @ 4^0C

   Record Primary:_____

5. 2 X 15 min Rinse with 1% BSA/PBS
6. 1 hour 5% Normal Serum (in 1% BSA/PBS)
7. ******COVER WITH FOIL*******
8. 48 hours *Secondary* (1% BSA/PBS [1:100]) shaking gently @ 4^0C

   Record Secondary: _____

9. 2 X 15 min Rinse with 1% BSA/PBS
10. 15 min Rinse with 0.01M PBS
11. 48 hours Phalloidin [1:50] in PBS shaking at 4^0C
12. 3 X 15 min Rinse with PBS
13. Overnight DAPI [1:5000] in PBS shaking at 4^0C
14. 15 min Rinse with 0.01 PBS

A.1.4 Expansion Protocol

A.1.4.1 Gelation

1. Prepare solutions (see attached chemical chart. Chemicals can be scaled up or down as needed)
    a. Acryloyl-X SE (AcX)/DMSO stock solution
    b. Monomer Solution (Stock X)
    c. TEMED stock solution
    d. Ammonium persulfate (APS) stock
    e. 4-hydroxy-TEMPO (4HT) solution
2. Replace sample buffer with 0.1 mg/ml Acryloyl-X SE (AcX) in PBS
3. Leave the tissues in AcX solution for >6 hours (overnight is fine) at room temperature with no shaking.

4. Construct gelation chamber

    a. Place two coverslips as spacers on the slide, separated from each other by 22 mm

    b. Use a thick and robust coverslip for the lid.

    c. Below is a schematic of the construction of the gelation chamber. This schematic comes from figure 4 in the 2018 Asano paper, *Expansion Microscopy: Protocols for Imaging Proteins and RNA in Cells and Tissues.*

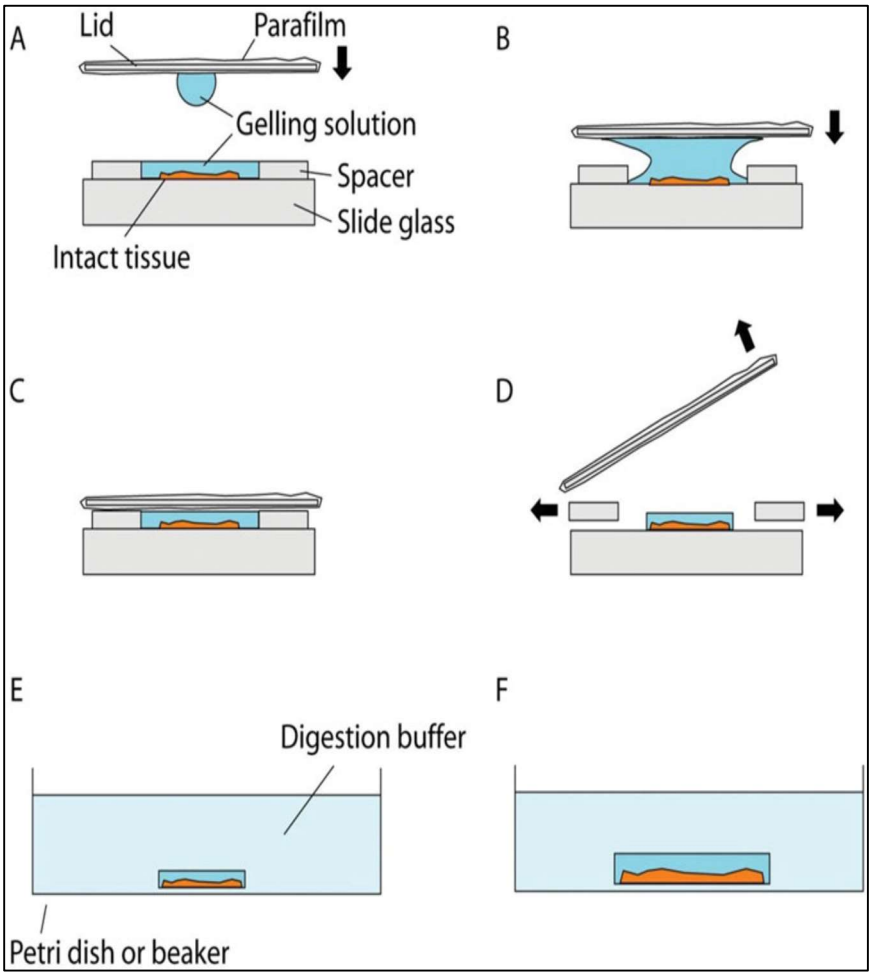

Figure A.1. Schematic for gelation chamber for gelling in-tact tissues. (Asano, 2018)

5. After incubating the tissues in the AcX solution, wash the tissues twice, each time for 15 minutes, with PBS.

6. Begin thawing the components for the gelling solution: Stock X, 4HT, APS with TEMED (keep the solutions chilled with an ice bath or on a cold block)
7. Add Stock X, 4HT, TEMED and APS in a 47:1:1:1 ratio in this order into a Microcentrifuge tube and vortex for a few seconds.
    a. Ensure the components consistently stay cold to prevent premature gelation
8. See attached Chemical Chart for amounts. Amounts can be scaled up or down as needed.
9. Add 500 um – 1 mL of gelling solution to fresh wells in the well plate.
10. Using a soft paintbrush, carefully transfer the tissue samples into the gelling solution.
11. Keep the plate the sample and the gelling solution at 4^0C, in the dark, for 30 minutes
    a. (complete next 3 steps within 5 minutes to prevent premature gelation)
12. Add a droplet of 60 - 80 µl of gelling solution in between the spacers, transfer the tissue to the droplet, and use the paintbrush to slowly flatten the tissue within the liquid environment. Gently press the tissue onto the glass surface.
13. Slowly lower a coverslip at an angle over the top of the tissue and spacers, make sure there are no air pockets trapped.
14. Using a pipette and a fine tip pipette, add gelling solution to both open sides of the chamber until the space between the lid, spacers, and slide is filled.
15. Place the gelation chamber in an incubator at 37^0C for 2 hours for polymerization.

A.1.4.2 Digestion

16. Take gelation chamber out of incubator
17. Slowly insert a razor blade, from the side, between the lid and the spacers, and pry the lid open. Once the lid is separated from the gel, remove the spacers in a similar fashion.
18. Trim any excess gel off using a razor blade.
19. Prepare digestion buffer (Add proteinase K to previously mixed digestion buffer base)

20. Use a paintbrush to wet the gel and its sides with digestion buffer base (without proteinase K). Let sit for 10 to 30 seconds (until the buffer soaks into the border).
21. Peel off the gel by gently probing the space between the gel and the glass surface with a fine paintbrush. Add 1 – 2 mL of the digestion buffer to one well of a 6-well plate for each sample and immerse the gel in the digestion buffer for > 8hours (overnight is fine) at room temperature, in the dark.

A.1.4.3 Storage and Expansion

22. Remove the digestion buffer and add PBS. Be careful not to suck up the gel while pipetting out the digestion buffer. This can be stored, in the dark, at 4 ^{0}C, if later imaging is desired.
23. Trim the gel, into an asymmetric shape, to the minimum size necessary. Remove any gel outside the region of interest (ROI). Transfer the ROI into a container that is large enough to contain the expanded gel. (expansion will add an additional 2X to 2.5X linear increase in size)
24. Place an imaging gasket upside down in a Petri dish.
25. Using a soft paintbrush, transfer the gel from the 6-well plate into the imaging gasket.
26. Fill the container with water, immerse the gel and allow it to sit for 20 minutes. After 20 minutes, replace the water with fresh water and wait 20 minutes. Repeat this step once more (for a total of 3 water changes).
27. Remove the excess water from the imaging gasket and mount the gasket on a slide.

A.1.4.4 Digestion

28. Take gelation chamber out of incubator
29. Slowly insert a razor blade, from the side, between the lid and the spacers, and pry the lid open. Once the lid is separated from the gel, remove the spacers in a similar fashion.
30. Trim any excess gel off using a razor blade.
31. Prepare digestion buffer (Add proteinase K to previously mixed digestion buffer base)

32. Use a paintbrush to wet the gel and its sides with digestion buffer base (without proteinase K). Let sit for 10 to 30 seconds (until the buffer soaks into the border).
33. Peel off the gel by gently probing the space between the gel and the glass surface with a fine paintbrush. Add 1 – 2 mL of the digestion buffer to one well of a 6-well plate for each sample, and immerse the gel in the digestion buffer overnight, or up to 2 days at room temperature, in the dark. *Note: For thick tissues: the ProK can be carried out for a longer time and/or at a higher temperature (up to 50 to 60^{0}C) depending on the biological composition and how strongly it is cross-linked after fixation. For a 250 μm thick mouse brain slice, a 2-day digestion at room temperature. The digestion buffer should be changed each day.

A.1.4.5 Storage and Expansion

34. Remove the digestion buffer and add PBS. Be careful not to suck up the gel while pipetting out the digestion buffer. This can be stored, in the dark, at 4 ^{0}C, if later imaging is desired.
35. Trim the gel, into an asymmetric shape, to the minimum size necessary. Remove any gel outside the region of interest (ROI). Transfer the ROI into a container that is large enough to contain the expanded gel. (expansion will add an additional 2X to 2.5X liner increase in size)
36. Place an imaging gasket upside down in a Petri dish.
37. Using a soft paintbrush, transfer the gel from the 6-well plate into the imaging gasket.
38. Fill the container with water, immerse the gel and allow it to sit for 20 minutes. After 20 minutes, replace the water with fresh water and wait 20 minutes. Repeat this step once more (for a total of 3 water changes).
39. Remove the excess water from the imaging gasket and mount the gasket on a slide.

A.1.4.6 Imaging

Choice of imaging technique, equipment, and objective can be made based on the desired experiment. For the purposes of this experiment the imaging was performed on the Zeiss LSM 510 system using the 20X and 40X water immersion lenses.

A.2 CHEMICAL LIST

Table A.2 Chemicals for use with Expansion Microscopy

Solution	Chemical	Amount
Stock Solutions	-	-
TEMED Stock Solution		
	TEMED	1.29 mL
	Water	1 mL
	Storage: Can be stored in 1 mL aliquots at -20^0 C 2 weeks	
APS Stock		
	APS	10g
	Water	100 mL
	Storage: Can be stored in 1 mL aliquots at -20^0 C 2 weeks	
4-hydroxy-TEMPO (4HT) Stock		
	4HT	0.5 g
	Water	100 mL
	Storage: Can be stored in 1 mL aliquots at -20^0 C for a month	
2-(N-morpholino)ethanesulfonic acid (MES) - buffered saline [MBS]	(for thick tissue protocol)	
	MES (100mM)	
	NaCl (150mM)	
	Water	
	*Adjusted to pH 6	
Acryloyl-X SE Stock Solution (AcX/DMSO)		

	Acryloyl- X SE	5 mg (or 10 mg for larger amount)
	DMSO	500 uL (or 1 mL for larger amount)
	Storage: Divide into 20 uL aliquots and store at -20 ^{0} C, in a sealed container with a drying agent. Can be stored for a month.	
Acryloyl-X SE Solution		[1:100]
	AcX/DMSO solution (10mg/mL)	20 uL
	PBS	1980 uL
Acryloyl-X SE Solution for thick tissues		[1:100]
	AcX/DMSO solution (10mg/mL)	20 uL
	MBS	1980 uL
Monomer Solution (Stock X)		
	Sodium acrylate (38 g/100 mL)	2.25 mL
	Acrylamide (50g/100 mL)	0.5 mL
	N,N'-Methylenebisacrylamide (2g/100mL)	0.75 mL
	NaCl (5M)	4 mL
	PBS (10X stock)	1 mL
	Water	0.9 mL
	Total	9.4 mL
	Storage: Can be stored in 1 mL aliquots at -20^{0} C for a month	
Gelling		
Gelling Solution (Intact Tissues)		
	Monomer Solution	188 uL
	4HT	4 uL
	TEMED	4 uL
	APS	4 uL
	Total	200 uL

Gelling Solution Thick Tissue Solution		
	Monomer Solution	188 uL
	4HT	6 uL
	TEMED	4 uL
	APS	4 uL
	Total	200 uL
	Storage: Gelling solution should be prepared at 4^0 C and used immediately. Right before vortexing and usage, APS should be mixed into the solution to prevent premature polymerization	
Digestion		
Digestion Buffer		
	Triton X-100	2.50g
	EDTA, disodium (0.5 M, pH 8)	1 mL
	Tris•CL (1M) aqueous solution, pH 8	25 mL
	NaCl	23.38 g
	Water	Fill container to 500 mL
	**Proteinase K (800 U/mL)	1:100 dilution
	Total	500mL

A.3 PREVIOUSLY USED FLUOROPHORES AND SAMPLE TYPES

Table A.3 Commercially available fluorophores used with expansion microscopy

Label	**Specimen Type**	**Reference**
Common Primary Antibodies		
anti-acetylated tubulin primary	kidney, giardia, drosophila	(Chozinski, 2018); (Halpern, 2017); (Jiang, 2018)
anti-actinin-4 primary	FFPE human, brain	(Bucur, 2016); (Gao, 2019)
anti-alpha smooth muscle actin primary	FFPE human, kidney	(Bucur, 2016); (Chozinski, 2018)

anti-alpha tubulin primary	kidney, cultured cell, planarian	(Chozinski, 2018); (Tsai, 2019); (Wang, 2016)
anti-bassoon primary	brain	(Burgers, 2019); (Chen, 2015); (Gao, 2019); (Tillberg, 2016); (Truckenbrodt, 2018)
anti-beta-galactosidase	drosophila	(Menon, 2019)
anti-Brunchilot	drosophila	(Min, 2019); (Jiang, 2018)
anti-C(3)C C-terminal primary	drosophila	(Cahoon, 2017)
anti-CaMKII primary	brain	(Chen, 2015)
anti-Caspr primary	brain	(Gao, 2019)
anti-ChAT primary	brain, drosophila	(Chen, 2015); (Mosca, 2017)
anti-clathrin heavy chain primary	chlamydomonas centrioles	(Gambarotto, 2019)
anti-collagen IV primary	FFPE human, kidney, brain	(Bucur, 2016); (Chozinski, 2018); (Gao, 2019)
anti-connexin primary	brain	(Crittenden, 2016)
anti-DsRed (tdTomato) primary	brain, drosophila	(Crittenden, 2016); (Jiang, 2018); Mosca (2017)
anti-GFAP primary	brain	(Burgers, 2019); (Crittenden, 2016)
anti-GFP primary	drosophila, brain, zebrafish, cultured cell	(Cahoon, 2017); (Crittenden, 2016); (Freifeld, 2017); (Gao, 219); (Jiang, 2019); (Kunz, 2019); (Lee, 2019); (Menon, 2019); (Min, 219); (Mosca, 2017); (Tillberg, 2016)
anti-HA primary	drosophila, brain, giardia	Cahoon, 2017); (Gao, 2019); (Halpern, 2017); (Mosca, 2017)
anti-homer primary	brain	Gao, 2019); (Lee, 2019); (Tillberg, 2016); (Truckenbrodt, 2018)
anti-Lamin A/C primary	brain	(Chen, 2015); (Tillberg, 2016)
anti-Lamin B1	cultured cell	(Min, 2019)
anti-MAP2	brain	(Min, 2019)
anti-MBP primary	brain	(Gao, 2019); (Min, 2019)
anti-MBP primary	brain	
anti-mCherry	cultured cell	(Kunz, 2019)
anti-mouse primary	cultured cell	(Min, 2019)
anti-NeuN	brain	(Artur, 2018); (Min, 2019)
anti-rabbit primary	cultured cell	(Min, 2019)
anti-rat IgG	cultured cell	(Kim, 2019)
anti-RFP	brain, drosophila	(Lee, 2019); (Menon, 2019)
anti-streptavidin	cultured cell	(Xu, 2016)
anti-synapsin	planarian	(Wang, 2016)
anti-synaptophysin	brain	(Truckenbrodt, 2018)
anti-synaptopodin	kidney	(Chozinski, 2018)
anti-Synaptotagmin	drosophila, zebrafish	(Min, 2019); (Freifeld, 2017)

anti-TOM20 primary	FFPE human, brain, chlamydomonas centrioles	Bucur, 2016); (Gao, 2019); (Tillberg, 2016); (Gambarotto, 2019)
anti-tubulin primary	zebrafish, arabidopsis thaliana, cultured cell	Freifeld, 2017); (Kao, 2019); (Truckenbrodt, 2018); (Zhang, 2106);
anti-vimentin primary	FFPE human, kidney, brain	Bucur, 2016); (Chozinski, 2018); (Gao, 2019); (Tillberg, 2106)
anti-α-actin	cultured cell	(Sheard, 2019)
anti-α-tubulin primary	FFPE human, chlamydomonas centrioles, cultured cell	Bucur, 2016); Gambarotto, 2019); (Grafe, 2019)
anti-β-tubulin	cultured cell	(Kang, 2019); (Min, 2109); (Tsai, 219)
DAPI	FFPE Human, kidney, planarian	(Bucur, 2018); (Wang, 2016)
Common Secondary Antibodies		
AlexaFluor 405	cultured cell	(Chozinski, 2016); (Min, 2019)
AlexaFluor 488	kidney, FFPE human, brain, drosophila, zebrafish, chlamydomonas centrioles, giardia, arabidopsis thaliana, cultured cell,	Bucur, 2018); (Bucur, 2016); (Burgers, 2019); (Cahoon, 2017); (Chen, 2015); (Chozinski, 2018); (Crittenden, 2016); (Freifeld, 2017); (Gambarotto, 2019); (Halpern, 2017); (Jian, 2018); (Kao, 2019); (Kim, 2019); (Kunz, 2019); (Lee, 2109); (Min, 2019); (Mosca, 2017); (Sheard, 2019); (Tillberg, 2016); (Truckenbrodt, 2018); (Tsai, 2019)
AlexaFluor 546	kidney, FFPE human, cultured cell, brain, zebrafish, drosophila, arabidopsis thaliana, chlamydomonas centrioles, arabidopsis thaliana	Bucur, 2018); (Bucur, 2016); (Chozinski, 2016); (Crittenden, 2016); (Freifeld, 2017); (Gao, 2019); (Kang, 2019); (Tillberg, 2016); (Truckenbrodt, 2018)
AlexaFluor 555	drosophila, arabidopsis thaliana	(Cahoon, 2017); (Kao, 2019)
AlexaFluor 568	brain, kidney, zebrafish, chlamydomonas centrioles, giardia, cultured cell, drosophila	(Burgers, 2019); (Chiozinski, 2018); (Freifeld, 2017); (Gambarotto, 2019); (Gao, 2019); (Halpern, 2017); (Lee, 2019); (Min, 2019); (Mosca, 2019)
AlexaFluor 594	cultured cell	(Tillberg, 2016)
AlexaFluor 633	brain	(Crittenden, 2016)

AlexaFluor 647	chlamydomonas centrioles, drosophila, cultured cell, brain	(Gambarotto, 2019); (Mosca, 2017); (Tillberg, 2016); (Xu, 2016); (Burgers, 2019)
AlexaFluor 647N	cultured cell	(Chozinski, 2016)
AlexaFluor 647N	brain, zebrafish, cultured cell	Chozinski, 2016); (Freifeld, 2017); (Gao, 2019); (Kunz, 2019); (Truckenbrodt, 2018)
AlexaFluor 680	cultured cell	(Sheard, 2019)
Atto 488	cultured cell, brain, kidney, giardia	(Chozinski, 2016); (Chozinski, 2018); (Halpern, 2017)
Atto 565	brain, cultured cell, giardia, drosophila	Chen, 2015); (Chozinski, 2016); (Halpern, 2017); (Jiang, 2018)
Atto 655	cultured cell, kidney, FFPE human, drosophila, brain, zebrafish	Sheard, 2019); (Bucur, 2018); (Bucur, 2016); (Cahoon, 2017); (Chen, 2015); (Chozinski, 2016); (Freifeld, 2017)
Biotin	cultured cell	(Chozinski,2016)
Biotin-conjugated goat anti-mouse IgG	cultured cell	(Tsai, 2019)
Biotinylated IgG	brain	(Crittenden, 2016)
CF405M/S	brain, cultured cell, zebrafish	(Lee, 2019); (Min, 2019); (Tillberg, 2016); (Freifeld, 2017)
CF430	cultured cell	(Min, 2019)
CF440	cultured cell	(Min, 2019)
CF450	cultured cell	(Min, 2019)
CF488A	brain, cultured cell	(Min, 2019)
CF514	cultured cell	(Min, 2019)
CF532	cultured cell	(Min, 2019)
CF543	cultured cell	(Min, 2019)
CF555	cultured cell	(Min, 2019)
CF568	cultured cell, brain	(Min, 2019); (Xu, 2016)
CF570	cultured cell	(Min, 2019)
CF583	cultured cell	(Min, 2019)
CF594	cultured cell	(Min, 2019)
CF633	FFPE human, zebrafish, brain, cultured cell, drosophila	Bucur, 2016); (Freifeld, 2017); (Gao, 2019); (Lee, 2019); (Min, 2019); (Mosca, 2017); (Tillberg, 2016); (Truckenbrodt, 2016)
CF640R	cultured cell, brain	(Min, 2019), (Lee, 2019); (Truckenbrodt, 2018)
CF660C	cultured cell	(Min, 2019)
CF660R	cultured cell, brain	(Min, 2019)
CF680	cultured cell	(Min, 2019)
CF680R	cultured cell	(Min, 2019)
CF750	cultured cell	(Min, 2019)
Dendra2	cultured cell	(Tillberg, 2016)

DyLight450	cultured cell	(Tillberg, 2016)
EZ-link NHS-PEG-4-Biotin	giardia	(Halpern, 2017)
FITC-conjugated secondary	drosophila	(Mosca, 2017)
Hoechst	cultured cell	(Chozinski, 2016)
Hoechst 33258	drosophila	(Jiang, 2018)
JaneliaFluor 549	cultured cell	(Sheard, 2019)
mEos2	cultured cell	(Tillberg, 2016)
mKikGR	cultured cell	(Tillberg, 2016)
PATagRFP	cultured cell	(Tillberg, 2016)
peroxidase-conjugated anti-mouse secondary	bacteria	(Lim, 2019)
STAR 580	chlamydomonas centrioles	(Gambarotto, 2019)
STAR RED	chlamydomonas centrioles	(Gambarotto, 2019)
SYBR Gold	cultured cell	(Chozinski, 2016)
Genetically Expressed Proteins		
YFP	brain	(Gao, 2019)
mCitrine	brain	(Gao, 2019)
mCherry	brain	(Gao, 2019)
TdTomato	kidney	(Kaverina, 2019)
EGFP	kidney	(Kaverina, 2019)
Thy1-YFP	brain	(Tillberg, 2016)

Table A.4 Species and Tissue types previously used with expansion microscopy

Species	**Tissue/Cell/Bacteria Type**	**Reference**
Bacteria	Chlamydomonas	(Gambarotto, 2019)
Bacteria	Dictyostelium	(Grafe, 2019)
Bacteria	Giardia lamblia	(Halpern, 2017)
Bacteria	Chlamydia trachomatis	(Kunz, 2019)
Bacteria	E. Coli	(Lim, 2019); (Zang2016)
Bacteria	Lactobacillus Plantarum	(Lim, 2019)
Bacteria	Acetobacter Tropicalis	(Lim, 2019)
Bacteria	Salmonella enterica	(Lim, 2019)
Bacteria	Bifodobacterium breve	(Lim, 2019)
Bacteria	Clostridium innocuum	(Lim, 2019)
Bacteria	Bacteroides ovatus	(Lim, 2019)
Bacteria	Bacteroides finegoldii	(Lim, 2019)
Bacteria	Acidaminococcus intestini	(Lim, 2019)
Bacteria	Parabacteroides disasonis	(Lim, 2019)

Bacteria	Cirtobacter	(Lim, 2019)
Cultured Cell	BS-C2	(Chang, 2017)
Cultured Cell	Mouse hippocampal neurons	(Chang, 2017), (Gao, 2018); (Tsanov, 2016)
Cultured Cell	HEK293	(Chen, 2015); (Tillberg, 2016); (Zang, 2016)
Cultured Cell	HeLa	(Chen, 2016); (Kunz, 2019); (Tillberg, 2016); (Tsai, 2019); (Tsanov, 2016); (Gao, 2018)
Cultured Cell	BS-C1	(Chozinski, 2016)
Cultured Cell	PtK1	(Chozinski, 2016)
Cultured Cell	U2OS	(Gao, 2018)
Cultured Cell	MDCKII	(Gao, 2018)
Cultured Cell	Rat hippocampal neurons	(Hafner, 2019); (Truckenbrodt, 2018); (Truckenbrodt, 2019)
Cultured Cell	Cos7	(Kim, 2019)
Cultured Cell	BS-C4	(Li, 2018)
Cultured Cell	BS-C3	(Min, 2019)
Cultured Cell	WM983b	(Rouhanifard, 2018)
Cultured Cell	Rat myocytes	(Sheard, 2019)
Cultured Cell	Mouse Embryonic Stem Cells	(Tsanov, 2016)
Cultured Cell	U2OS	(Wang, 2018)
Cultured Cell	Mouse Spermatocytes	(Xu, 2016)
Cultured Cell	NIH/3T3 Fibroblasts	(Zhang, 2016)
Drosophila	Brain	(Cahoon, 2017); (Gao, 2019); (Jiang, 2018); (Menon, 2019); (Mosca, 2017); (Wang, 2018)
Drosophila	Embryos	(Tsai, 20017)
FFPE Human	Kidney	(Bucur, 2018); (Chozinski, 2018); (Klimas, 2019); (Zhao, 2017)
FFPE Human	Brain	(Deshpande, 2017)
FFPE Human	Various Cancerous Tissues (Undisclosed in article)	(Bucur, 2016)
FFPE Human	Breast	(Zhao,2017)
FFPE Human	Lymph Node	(Zhao,2017)
FFPE Human	Skin	(Zhao,2017)
FFPE Human	Liver	(Zhao,2017)
FFPE Human	Lung	(Zhao,2017)
FFPE Human	Prostate	(Zhao,2017)
FFPE Human	Pancreas	(Zhao,2017)
FFPE Human	Ovary	(Zhao,2017)
FFPE Human	Colon	(Zhao,2017)

Mouse	Brain	(Artur, 2018); (Burgers, 2019); (Chang, 2017); (Chen, 2015); (Chen, 2016); (Chozinski, 2016); (Crittenden, 2016); (Gao, 2017); (Gao, 2019); (Hafner, 2019); (Kang, 2019); (Karagiannis, 2018); (Lee, 2019); (Min, 2019); (Tillberg, 2016); (Wassie, 2019); (Zhang, 2016)
Mouse	Kidney	(Chozinski, 2018)
Mouse	Kidney	(Kaverina, 2019)
Mouse	Retina	(Saka, 2019)
Planarian (worm) Schmidtea Mediterranea	Neurons	(Wang, 2016)
Plants	Arabidopsis thaliana	(Kao, 2019)
Rat	Brain	(Truckenbrodt, 2018); (Truckenbrodt, 2019)
Zebrafish	Brain	(Freifeld, 2017)
Zebrafish	Whole Larval	(Kang, 2019)